STAR R & D Measurements With A Small Pad Test Chamber

H.Z. Huang, B.C. Stringfellow, J. Mooney, A.S. Hirsch, E. Hjort, N. Porile, R.P. Scharenberg, B. Srivastava, M. Tincknell

High Energy Nuclear Group, Purdue University

H. Wieman, A. Sobel

Nuclear Science Division, LBL

1 Introduction

The STAR TPC has an inner radius of 0.5 m, an outer radius of 2 m and a longitudinal length of 4.2 m. Ionization electrons drift towards both end caps of the TPC with a maximum drift length of 2.1 m. The two readout end caps are divided into an equal number of inner and outer sectors, 48 sectors in total. Because of the high multiplicity environment at RHIC ($dN/d\eta \sim 2000$ including secondary particles) and the large variation in particle density from inner radius to outer radius, two sizes of pads are necessary for the readout sector. These pads measure 2.85 mm $\times$ 11.5 mm for the inner sectors and 6.2 mm $\times$ 19.5 mm for the outer sectors.

The small pads will increase the two-track resolution, which is crucial in a high multiplicity environment in order to obtain hit position and dE/dx measurements. Because of the reduced pad size the gap between the anode plane and the pad plane has to be reduced from 4 mm for large pads to 2 mm for small pads, in order to obtain a pad response function covering three pads. The gap between anode plane and the ground plane is kept at 4 mm for easy sector construction (new calculation of wire deflection due to electrostatic force calls for symmetrical electrodes). These asymmetrical electrodes lead to a special sector geometry, which has not been used in previous TPC experiment. Extensive measurements are required to test this pad geometry.

Our goal is to establish the feasibility of the small pad readout scheme, to measure the characteristics of the prototype pad chamber for its gain variations, pad response functions and intrinsic resolutions. For this purpose the Purdue group established a testing lab at Purdue and has performed an extensive test of the pad chamber since January 1993. We report here on the test results.

2 Experimental Setup

The small pad prototype chamber was constructed at LBL. Figure 1 shows a top view of the chamber where the four curved pad rows can be seen. Figure 2 shows a schematic drawing of the chamber; the gaps between planes and characteristics of wires are also listed. Both anode and pad signals are read out. The anode signals are connected to an ORTEC 109 preamplifier through a switch board, then amplified again with a typical shaping time of 250 ns. The amplitudes of the anode signals are recorded using a digital scope or multichannel analyzer.

The pad signals are read out using the EOS-TPC DAQ system. A flat cable connects the pad connector to an EOS stick electronics. The stick contains 120 channels of preamplifiers, shaping amplifiers, switching capacitor arrays, analog digitalization and one fiber optical data transmission link. Digital data is sent to a receiver host in a VME crate via fiber optical links. A UNIX based data acquisition system (developed by C. MacParland and his group), running on a VME CPU (Motorola 147) and controlled by a SPARCstation via Ethernet, is used in our test setup. Figure 3 shows a schematic diagram of this setup.

3 Gain Measurement

One unique feature of the small pad readout is the reduced gap of 2 mm between the anode and pad planes resulting in an asymmetric electrostatic potential around the anode wires. Since gas gain depends strongly on the geometrical arrangement of anode, field, ground and pad planes, the gain uniformity requirement leads to strict tolerances for such things as wire placement, wire tension, inter-plane distances and planarity. Both the gain uniformity and wire placement accuracy have been studied.

An Fe^{55} source, which emits X-rays of 5.9 KeV, is used to measure the gas gain of the chamber. The number of electrons from the primary ionization is about 220. The anode signals from the shaping amplifier are analyzed using a multichannel analyzer. Both the initial X-ray peak and the escape peak resulting from Argon can be observed. The electronic system is calibrated by signals from a precise capacitor injected with a known amount of charge.

Figure 4 shows the gain as a function of anode high voltage for wire number 14 and 27 at both the center and the edge of the wires. The curves are exponential fits to the data. Typical operating voltage for the small pad readout is about 1200V.

For gain uniformity study, we have measured the relative gains of a total of 33 anode wires. Figure 5 shows the gain measurement at both ends of these wires. The variation (σ_g/g) is less than 1.5%. Figure 6 shows the gain variation along wire number 27 (near center). Again the σ_g/g is less than 1.5%. Thus, the gain uniformity is better than 1.5% over most of the active volume of the pad chamber.

Systematic errors in wire placement could lead to a systematic shift in gain. To look for such effects, the (x, z) positions of each wire (at both ends of the chamber) were measured by John Wolf at LBL. Figure 7 shows the z position (perpendicular to anode plane) distribution at each end of the chamber with a σ less than 15 microns. The x position deviation in the anode plane assuming an absolute pitch of 4 mm is not a Gaussian. The average deviation in x is about 50 microns with a maximum of about 100 microns. We do not observe any correlation between the gain variation and the geometrical deviations.

4 Pad Response Function Measurements

The pad response function (PRF) is defined as the amplitude of the pad signal as a function of the distance of the avalanche from the center of the pad. It depends on the pad geometry (size and orientation with respect to wire), as well as on the induced charge distribution from the avalanche (determined by the gap and capacitive coupling between anode and pad planes). The laser setup was used in the PRF measurement. The Nitrogen laser (VSL-337 from Laser Science, Inc.), triggered by an external pulse, was focused onto an Al-coated quartz window. Due to the unevenness of the window surface and the space charge from positive ions leaking into the drift region, there are large variations, up to 30–50%, in the amplitude of the anode signals, and consequently in the pad signals. To eliminate this effect the anode signal amplitude is read out by a digital scope and used to normalize the pad pulse height.

Figure 8 shows the pad response function parallel to the anode wires for pad channels 63, 64 and 65. These correspond to the fourth, fifth and sixth pad from the readout end of the middle short pad row, where there in no significant curvature with respect to anode wires. The lines are Gaussian fits to the measurements with a sigma of about 2.2 mm. The pad response function along the anode wires is generally considered a Gaussian distribution, to a good approximation. Theoretical calculations by Gatti *et al.*[1] and subsequent approximate parametrization by Mathieson[2] indicate a slight deviation from Gaussian. Early measurements by Fancher and Schaffer[3] have shown a deviation at the level of a few percent of the PRF amplitude. Figure 9 shows the residual from subtracting a Gaussian fit from the data. The dashed lines are the PRF data scaled by 3.4%. Note that both measurements with wide pads (7.5 mm width) by Fancher *et al.*[3] and by Sobel *et al.*[4] indicated a dip in the residual distribution at the middle of the pad. However, our measurement with narrow pads (2.85 mm width) indicates a small peak in the residual at the center of the pad.

The pad response function perpendicular to the anode wire is expected to be several steps across because the avalanche position is localized on each anode wire with a constant pitch of 4 mm. However, due to a finite laser size and diffusion in the gas the edge of each step would be smoothed. Figure 10 shows the PRF perpendicular to the anode wires for pads in the straight section of the pad row (near the readout end). The slight asymmetry of both sides of the PRF is due to small offset between wire pitch (4 mm) and pad length (11.5 mm). the shape of the PRF for two neighboring pads is very similar to that of the central pad; a small difference at the edges may be due to the fact that the PRF is not completely decoupled in X (perpendicular to wire) and in Y (parallel to wire) directions.

The PRF for straight pad rows versus curved pad rows has also been studied. This is important for high momentum particles which have little bending inside the TPC volume. For straight pad rows these particles from the interaction vertex have an incident angle up to 15 degrees with respect to the pad row. Figure 11 shows the PRF for pads from a straight section of the row, when the incident angles between the laser scan and the direction perpendicular to wire are 8 and 15 degrees respectively. There is a strong asymmetry in the PRF between the two neighboring pads. Thus for a traversing particle which produces avalanches on all anode wires along the path, the Landau fluctuation in the ionization could significantly deteriorate the accuracy of position measurement.

For circular pad rows, however, the PRFs for high momentum particles from two neighboring pads are approximately symmetrical. Figure 12 shows the PRF measurement when the laser scans radially. Thus in this geometry the effect of the Landau fluctuation in the ionization could be reduced.

Concerns were raised for the circular pad rows that the coupling between anode and pad will be strongly position dependent, which could compromise the dE/dx measurement. Simulations showed that the improvement due to circular pad rows in momentum resolution for high momentum particles is marginal. Therefore, there is little gain in the physics capability of the STAR TPC by using circular pad rows. The decision will largely be based on convenience in sector manufacture.

5 Resolution Measurement

The geometrical choices of pad size and gap width are determined by the position resolution and two track resolution. These resolutions are also coupled to the signal-to-noise ratio of the pad readout electronics. We studied the intrinsic position resolution of the small pad chamber for signal-to-noise ratios ranging from 200 to 400. The laser scan is performed parallel to the anode wire, and the position of the laser is calculated using signals from three or two pads. The variation of the position reflects the intrinsic resolution associated with the pad geometry. The resolution due to systematic errors is studied by comparing the calculated position versus scan position over many pads.

The avalanche position can be calculated from three or two pads. For the three pads case, the measured signal amplitudes are considered parts of the Gaussian pad response function

(PRF). The sigma of the PRF is $\sigma = g/(\log(h_2^2/h_1/h_3))^{1/2}$, where $h1$, $h2$ and $h3$ are signals from pad number 1, 2 and 3, and g is the pad pitch (3.35 mm). The position of the avalanche can be deduced from the Gaussian PRF: $x = \sigma^2 \log(h_3/h_1)/(2g) + g/2$. For the two pad case, the Gaussian PRF is not defined by the two pads. We must assume the σ of the Gaussian PRF (2.15 mm). Then the position can be calculated as $x = \sigma^2 \log(h_2/h_1)/g + g$.

Figure 13 shows the measured width σ in mm as a function of laser position. The σ reaches a minimum in the middle of the pad and increases by 150 microns at the edge of the pad. To understand this modulation we recall that the pad response function we have measured is not exactly Gaussian. There is a deviation from the Gaussian up to 3.4%. Using a function that was suggested to describe the induced charge distribution on the pad plane[3], we obtained a better fit to the measured PRF. The calculated σ from this fit is shown in figure 14 as a function of the avalanche position. We reproduced the essential feature and magnitude in the σ variation.

Figure 15 shows the calculated position (top panel), the position resolution (σ, not to be confused with that for the width of PRF) (middle panel) and the position deviation (bottom panel) as a function of the laser position for the three pad fits. The intrinsic position resolution with a signal-to-noise ratio of 200–400 for this pad geometry is about 40 microns. The position accuracy including systematic errors is about 100 microns. The modulation in the position deviation is due to the non-gaussian nature of the PRF.

The effect of this non-gaussian nature of the PRF is greatly amplified in the two pad fits. Figure 16 shows the calculated position, the position resolution and the position deviation as a function of the laser position using two pad fit. The width of the PRF, σ, has been fixed at 2.15 mm. Note there is a discontinuous jump in the position calculation at the center of the pad, where the pad numbers used for the two pad fit change. This can be attributed to the non-Gaussian nature of the PRF. Figure 17 shows the expected deviation for the two pad fit as a function of the laser position. Both the shape and the magnitude are consistent with our observation. The gain variation in the electronics of the pad readout system could contribute to additional smearing in the measured data.

The resolution measurements for the curved sections of the pad rows yielded similar results as shown in figures 13–16.

6 Two-track Resolution Measurement

We studied the intrinsic two-track resolution of the pad chamber using several laser beams. A splitter box from Laser Science, Inc. with one fiber for input laser beam and seven fibers for output beams was used to generate two signals. To reach the minimum distance of separation, we removed the focus lense. The laser spots should still be in the range of several hundred microns since the diameter of the fiber is only 200 microns.

Given a pad geometry, the two-track resolution depends on the relative signal strength, signal-to-noise ratio and the algorithm to calculate the hit positions. For the three pad fit there is no ambiguity in selecting which three pads to use. However, for two pad fit we have to decide which two pads to use for the fit since one avalanche normally induces signals on three pads. Current analysis was based on visual examination of the pulse amplitude from all pads: normally two pads with the largest signals were used in fit, but when two lasers were close to each other two pads away from the other laser were used. This procedure can be optimized, but the results presented here remain essentially the same.

Figure 18 shows the lego profile of the pad amplitude as a function of separation between two signals. At the starting point of about 13 mm apart, signals from two lasers are clearly separated. However, as the two lasers approach a distance of 6 mm apart there is only one broad peak in the pad signals. This scan was performed along the anode wire in the straight section of the pad row. The signal of the fixed laser is about 70% of the moving laser.

Figure 19 shows the calculated positions for the fixed laser. The jump in the two pad fits is due to the non-Gaussian nature of the pad response function, which has been discussed in the previous section. This jump also indicates the position where different sets of two pads were used in the fitting. The calculated positions from two pads are within 300 microns to the actual position for laser separation down to 6 mm. This constant offset could probably be corrected for by using a more accurate description of the pad response function. However, for three pad fits the position deviation increases as two lasers approaching each other. The deviation reaches more than 1 mm for laser separation less than 6 mm. Figure 20 and 21 show the calculated position and deviation as a function of laser separation for the moving laser. In this case, the modulations in the position accuracy discussed in the previous section are also noticeable.

This measurement indicates that for the small pad geometry we can measure track positions for two tracks as close as 6 mm. However, the two-track resolution for dE/dx measurement (three pad fits) is close to 10 mm. This is consistent with out expectations from initial design considerations for the small pad geometry.

Figure 22–25 show the two-track resolution measurement for two lasers with very different strength. In this case, the track position of the weak laser cannot be determined well for laser separation below 9 mm. Therefore, the two-track resolution for both position and dE/dx measurement is about 10 mm.

7 Conclusions

We have measured the characteristics of the small pad geometry. The pad response function has a width, σ, of about 2.15 mm, suitable for accurate position measurements. We have achieved an intrinsic position resolution of 40 microns and a systematic position resolution of about 100 microns. The two-track resolution for position measurements is about 6 mm and that for dE/dx measurements is about 10 mm when measured with lasers of equal intensities. The two-track resolution for position measurement approaches 10 mm when two lasers with greatly different intensities were used. The successful operation of this pad chamber proves the feasibility of the small pad design for inner sectors of the STAR TPC.

8 Acknowledgement

We thank Fred Bieser of LBL for much help during the course of this work. C. MacParland and J. Schambach provided assistance in initial DAQ setup for the Purdue testing lab.

References

[1] E. Gatti, A. Longoni, H. Okuno and P. Seemenza, Nucl. Inst. Meth. 163.

[2] E. Mathieson, Nucl. Inst. Meth. A270 (1988) 602.

[3] D.L. Fancher and A.C. Schaffer, IEEE Transactions on Nuclear Science, NS-26 (1979), 150.

[4] A. Sobel, E. Hjort, H.Z. Huang, P. Jones, J. Mitchell and H. Wieman, STAR Note # 88 (1992).

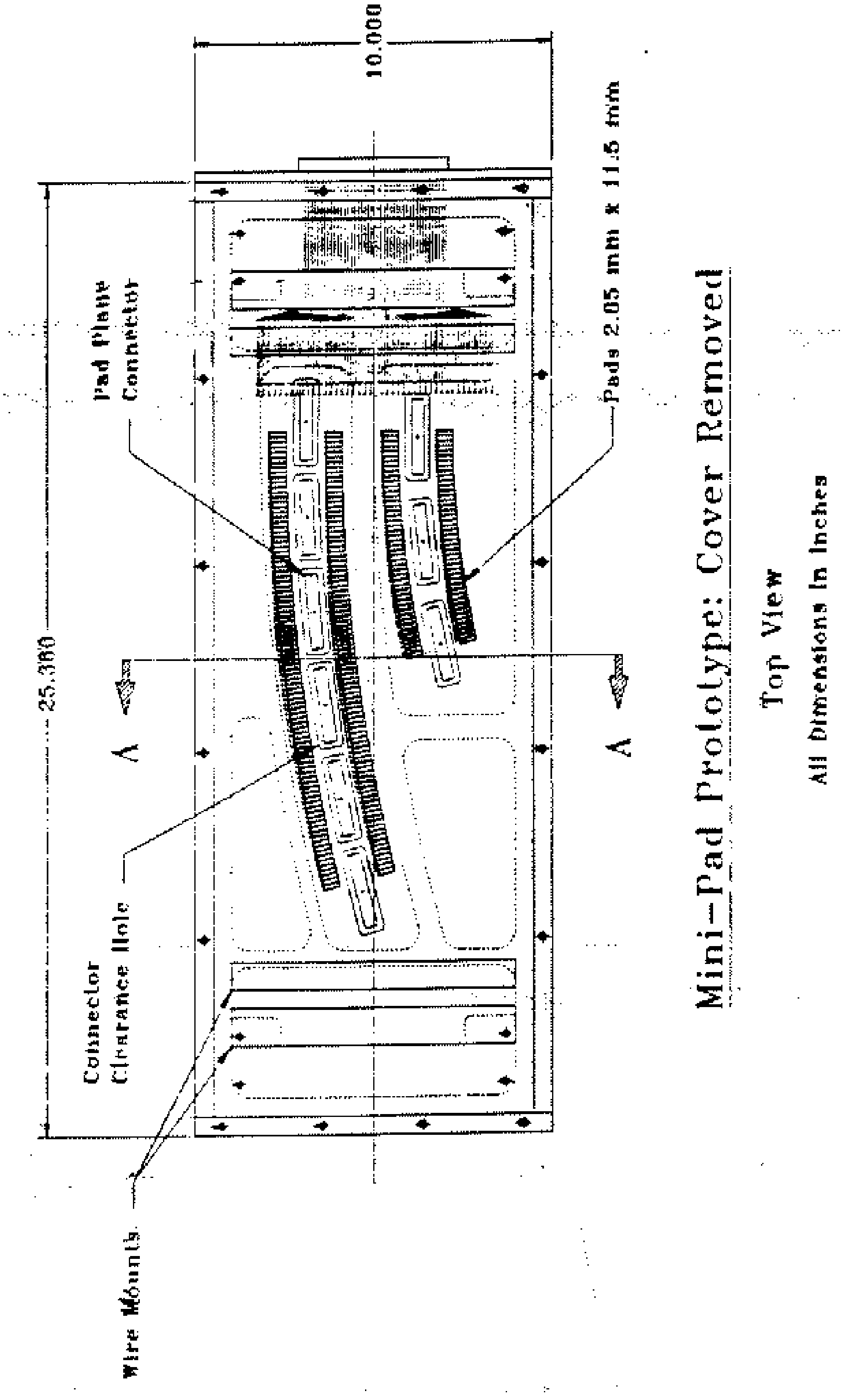

Figure 1: Top view of the pad chamber. Shown are four curved pad rows and wires.

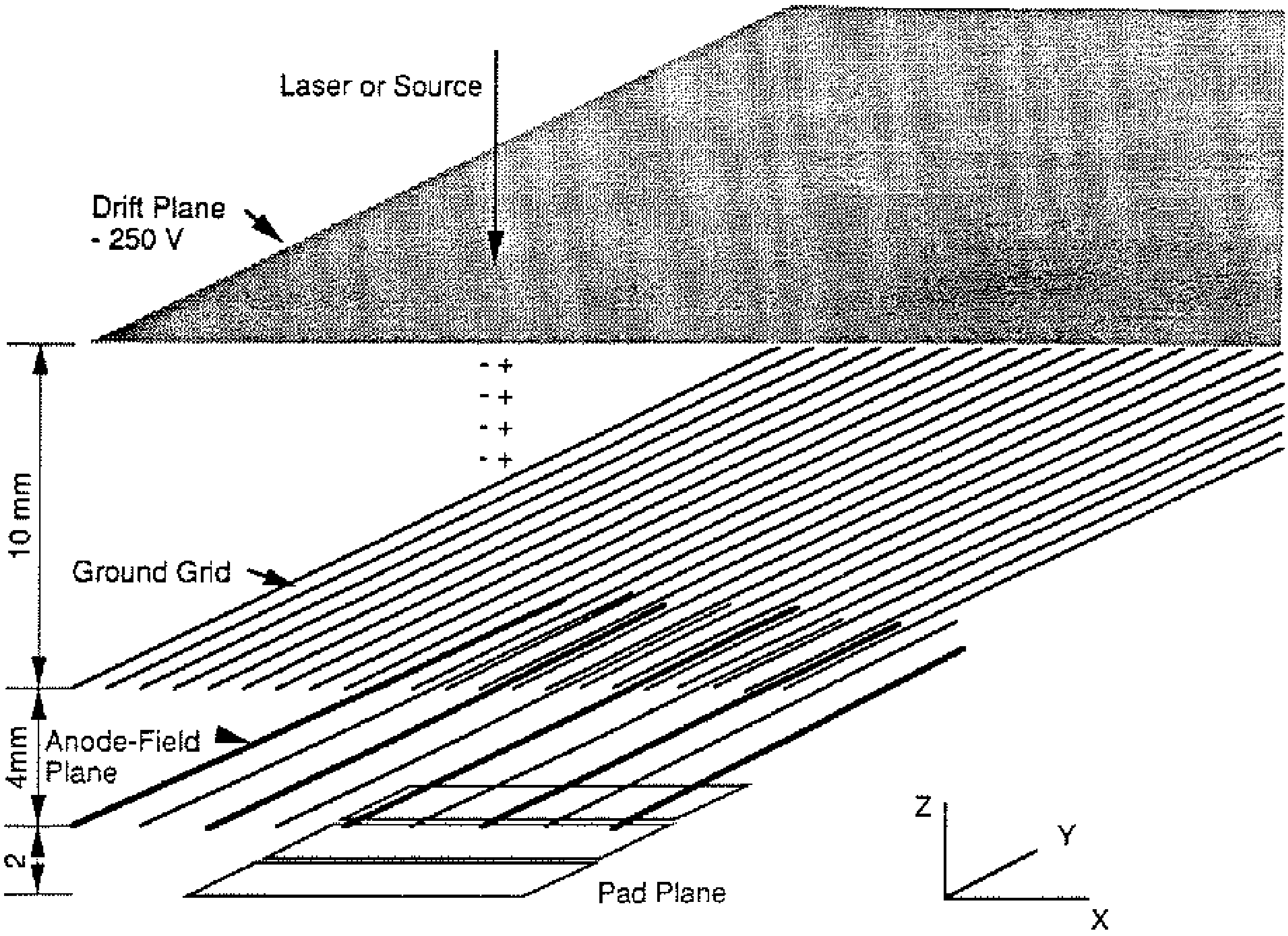

Drift Plane: ⇨ For Fe 55 Measurements - Mylar window with conductive TiO on inside

⇨ For Laser - Quartz Window with Al coating on inside -250 V

Field Wires: Ground Potential ϕ = 125 μm, Be-Cu

Anode Wires: +HV, ϕ = 20 μm, gold-plated tungsten

Pad Plane: 2.85 X 11.5 mm Pad
3.35 mm pitch
Curved Pad Rows

Gas: 90% Ar - 10% Methane

Figure 2: Schematic drawing of the pad and wire planes. Characteristics of wires and planes are listed.

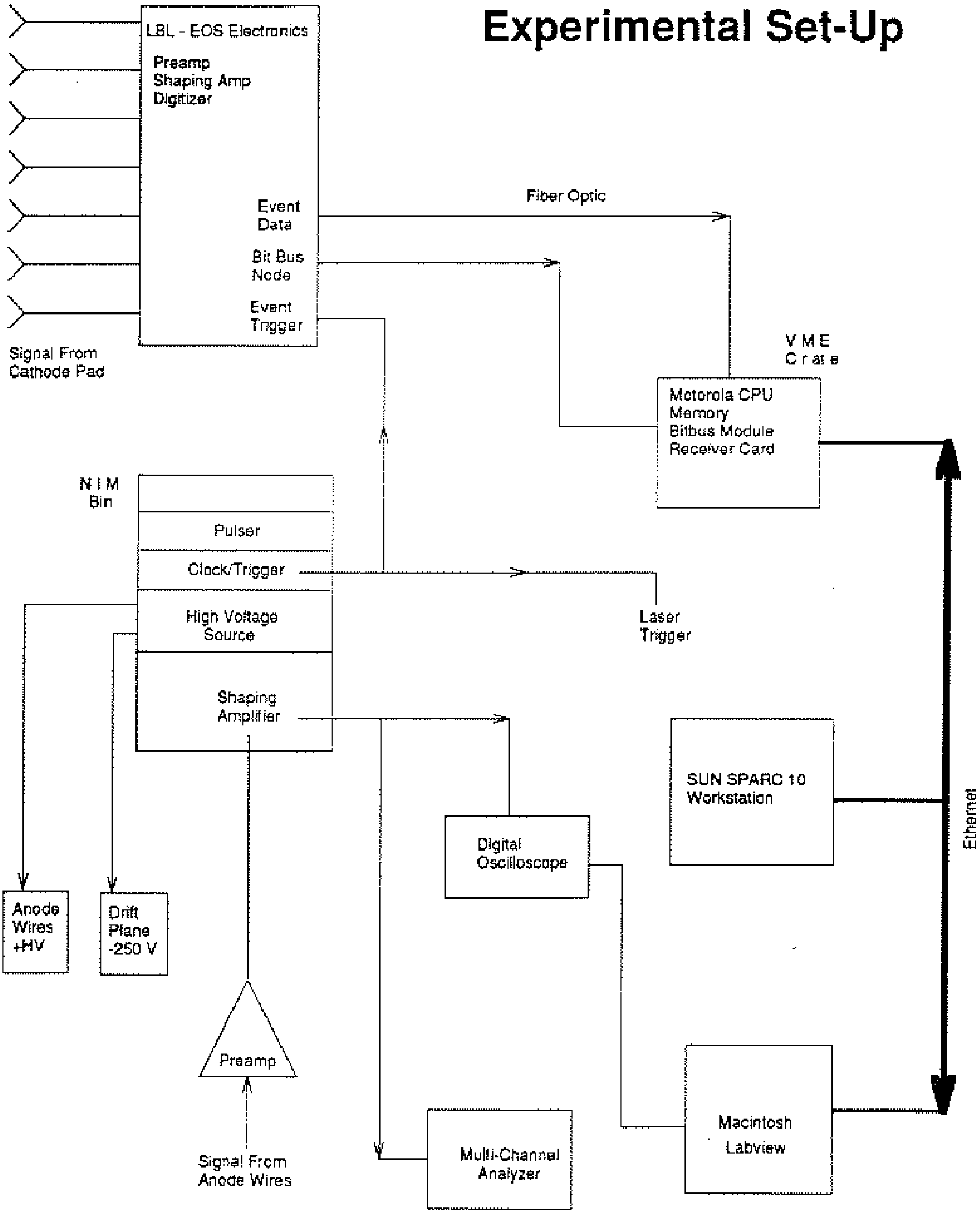

Figure 3: Schematic diagram of the testing setup.

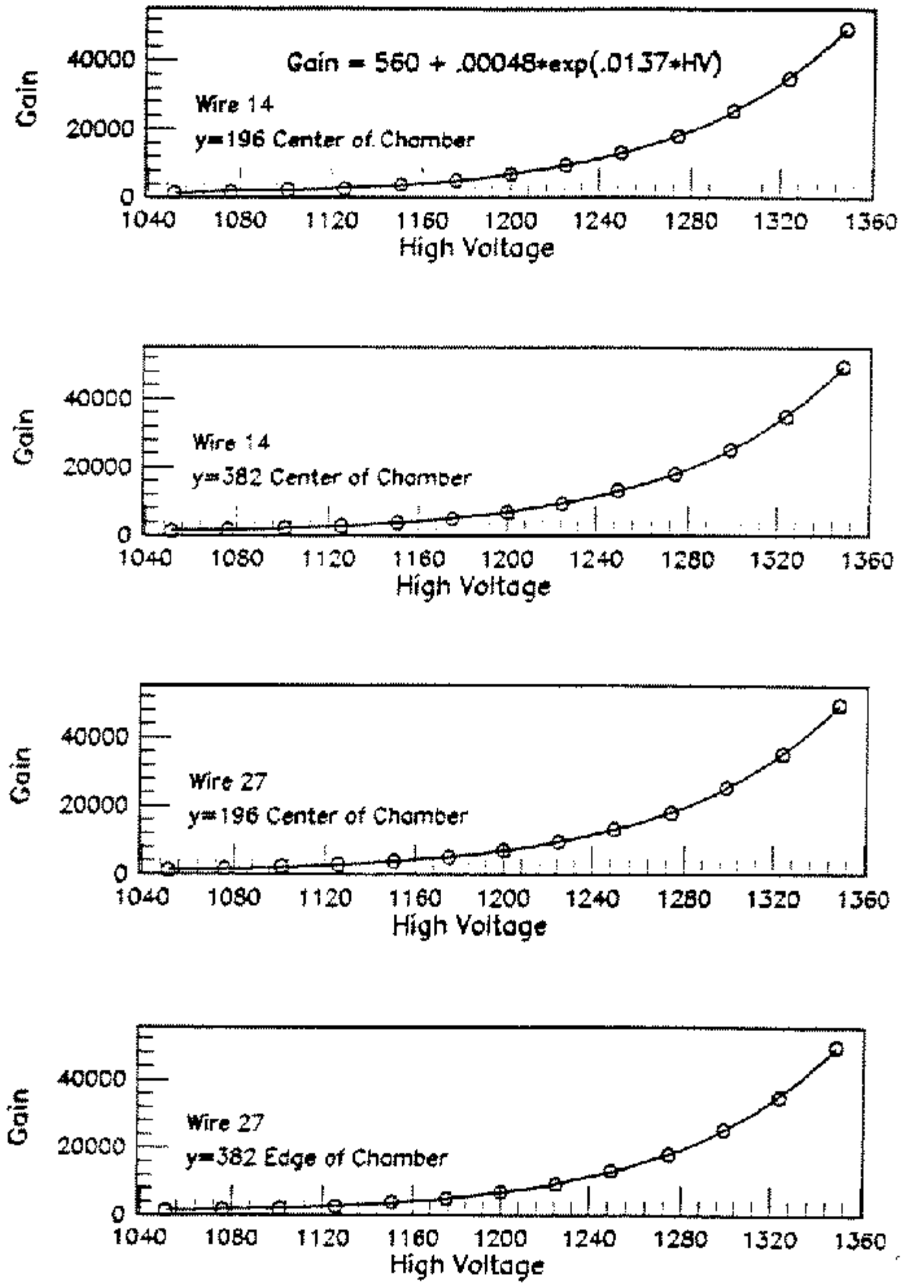

Figure 4: Gain as a function of anode high voltage. The curves are exponential fits.

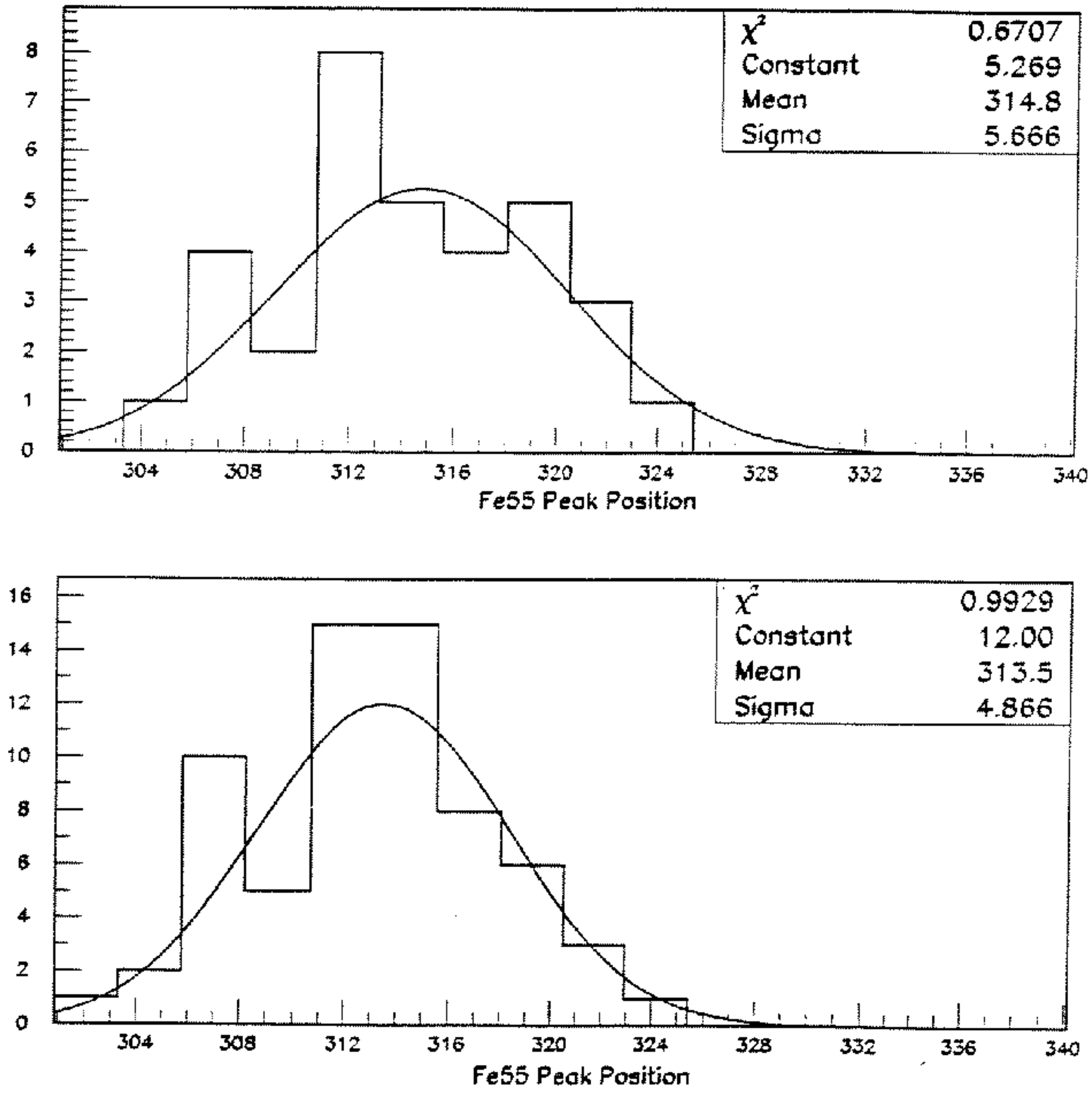

Figure 5: Relative gain measurement at both ends of the anode wires.

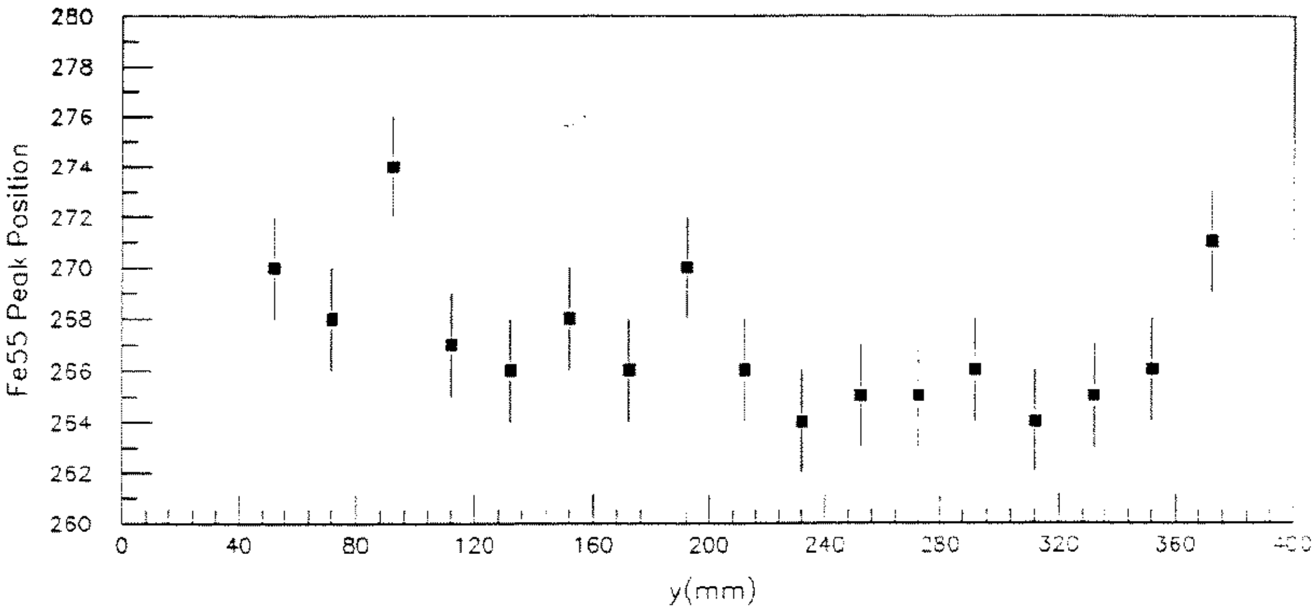

Figure 6: Gain variation along one anode wire.

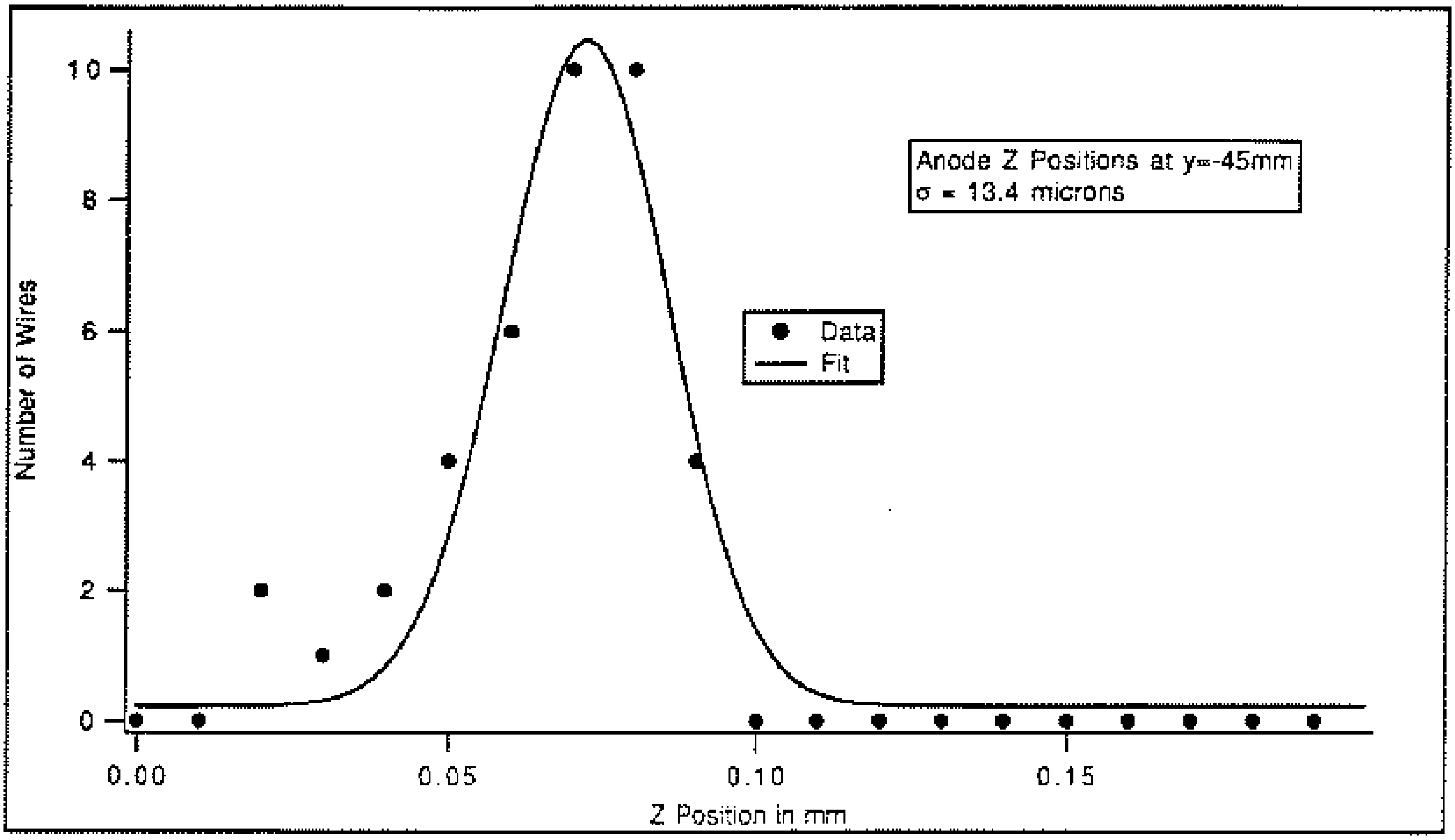

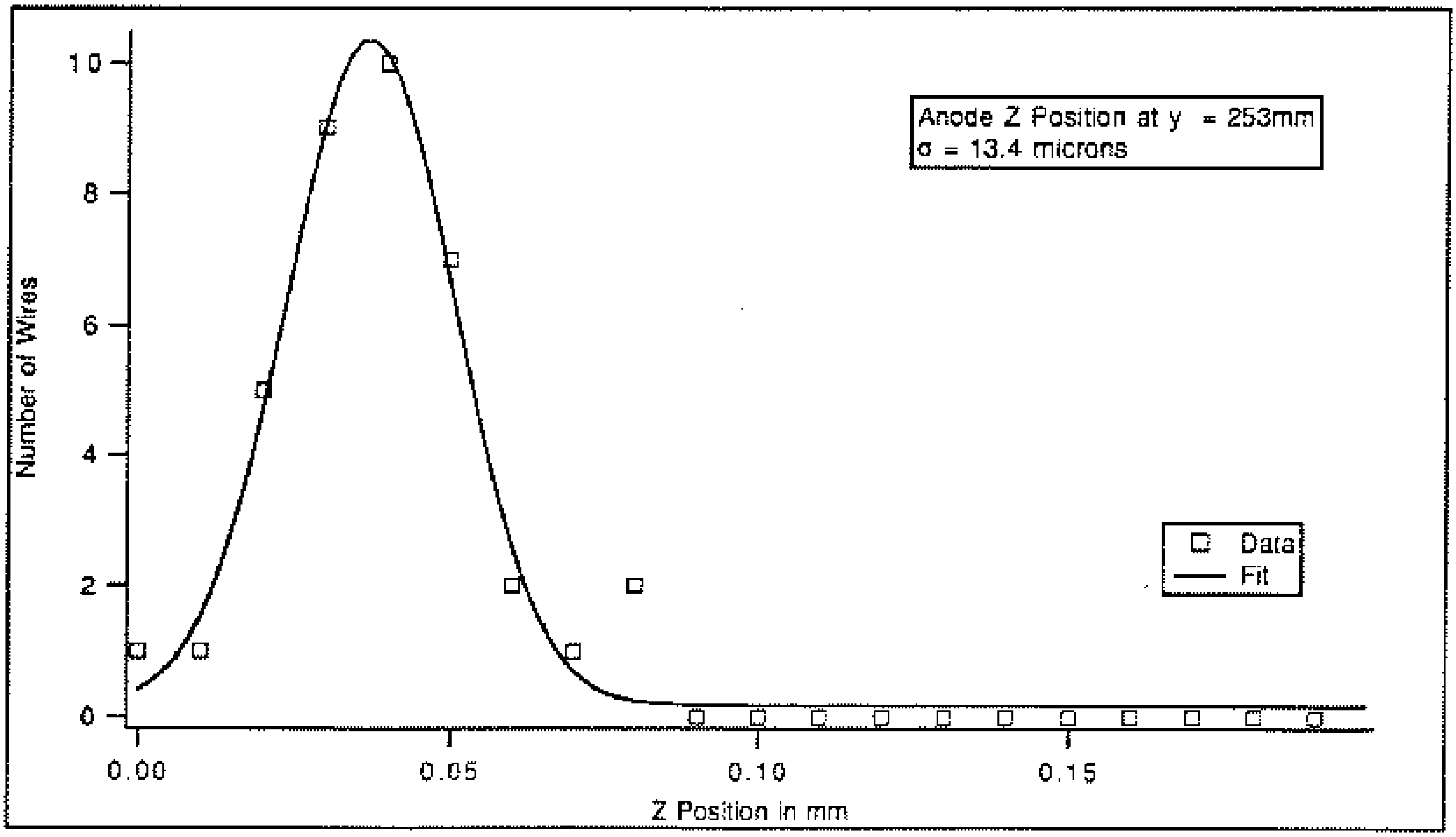

Figure 7: Z position distribution (perpendicular to anode plane) at each end of the chamber.

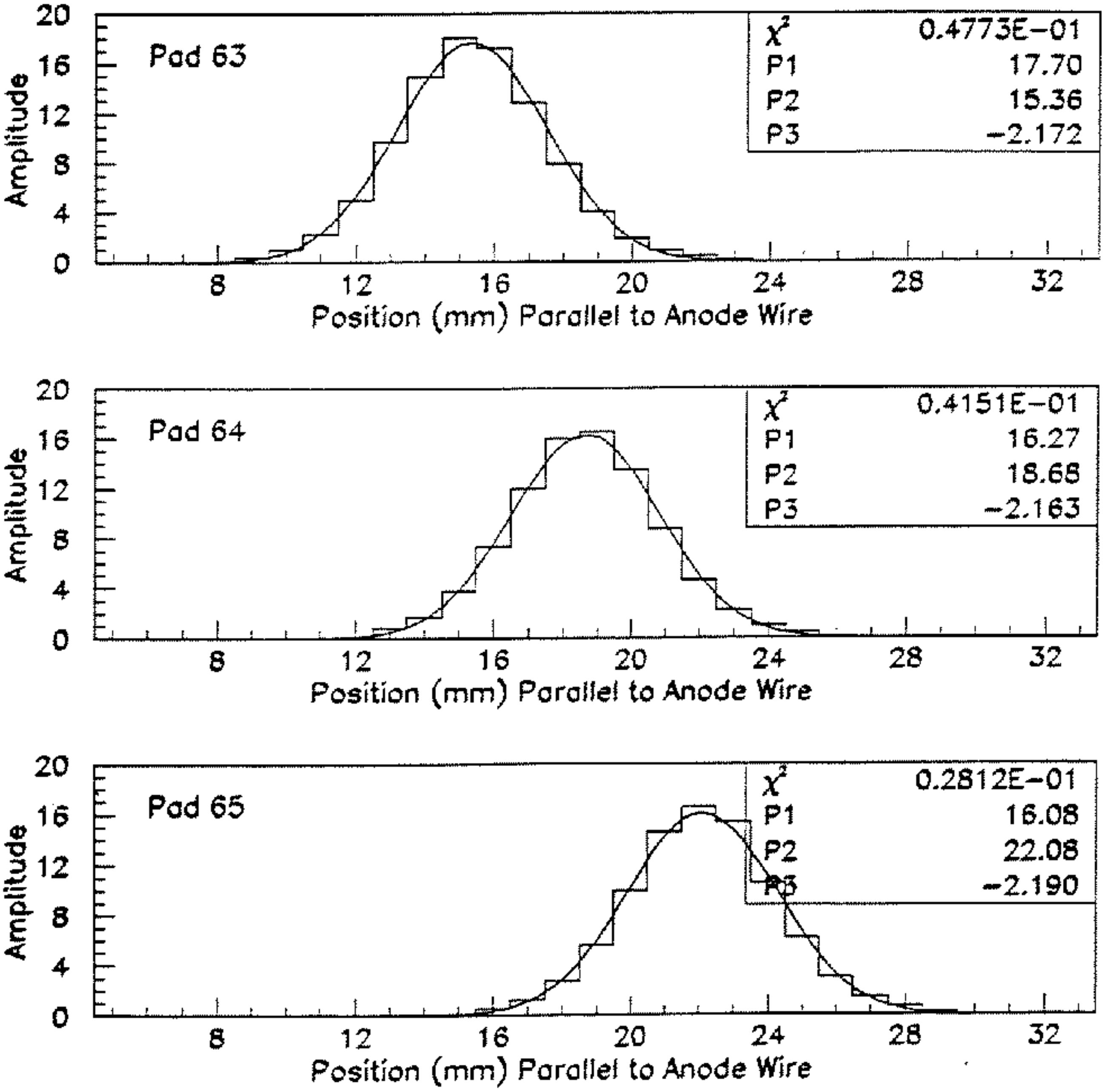

Figure 8: Pad response function parallel to the anode wires for pads at the straight section of the second row.

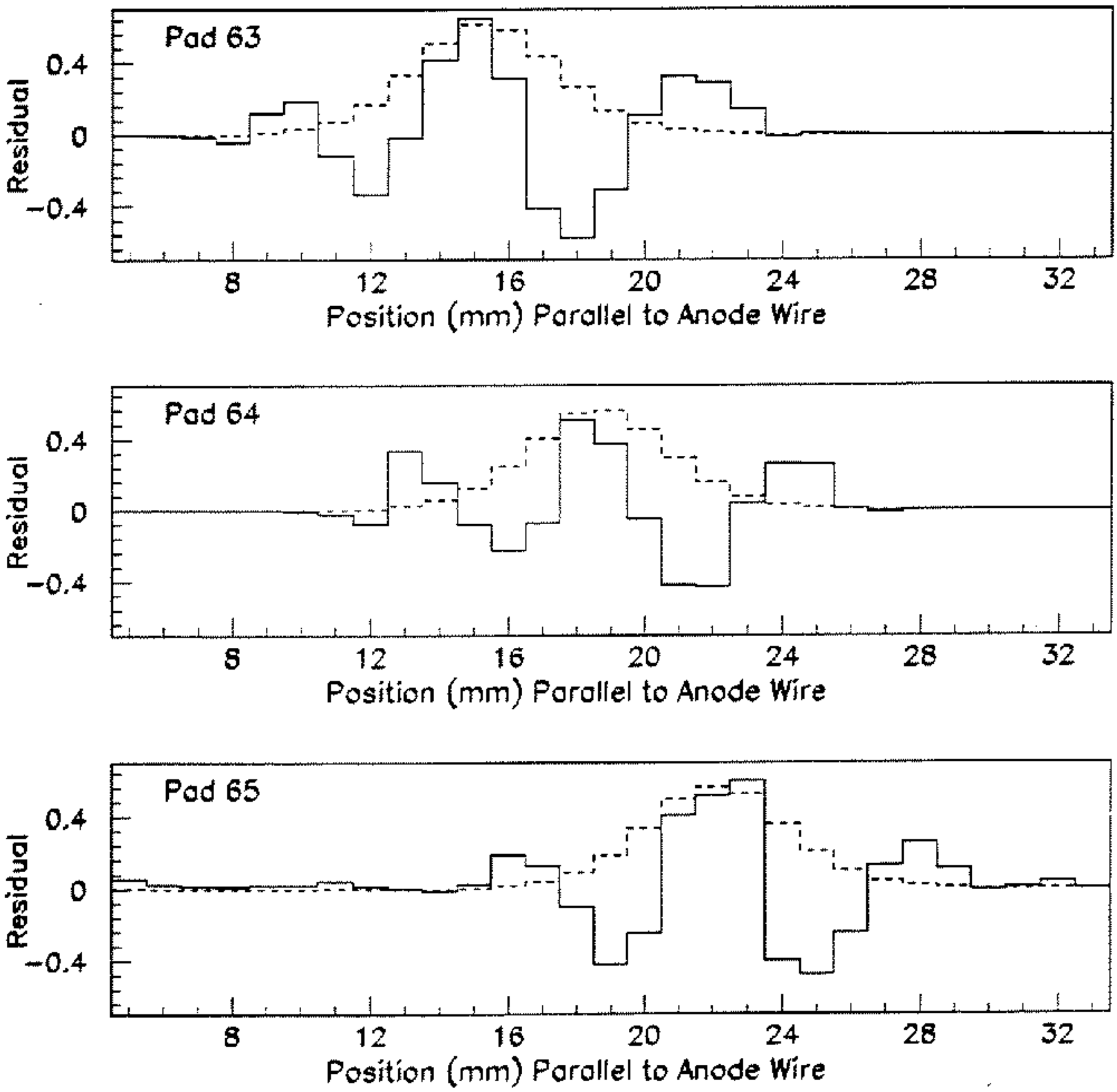

Figure 9: Residual of pad response function subtracted by Gaussian fit.

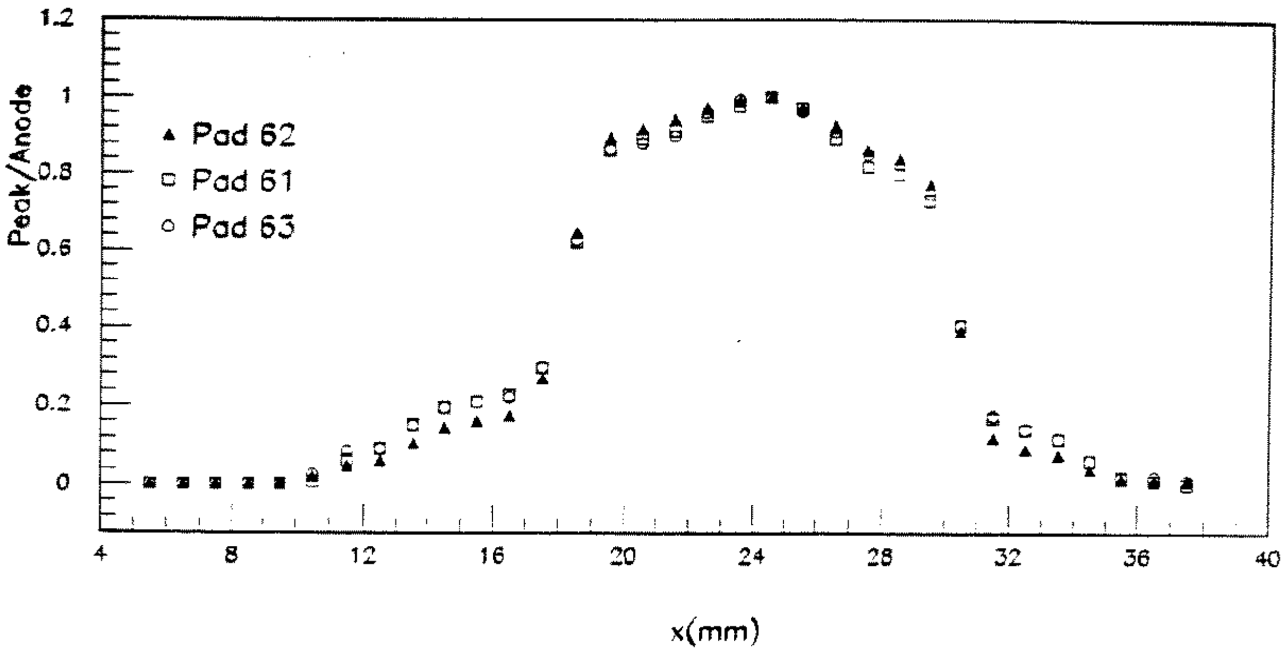

Figure 10: Pad response function perpendicular to the anode wires for pads in the straight scetion of the pad row.

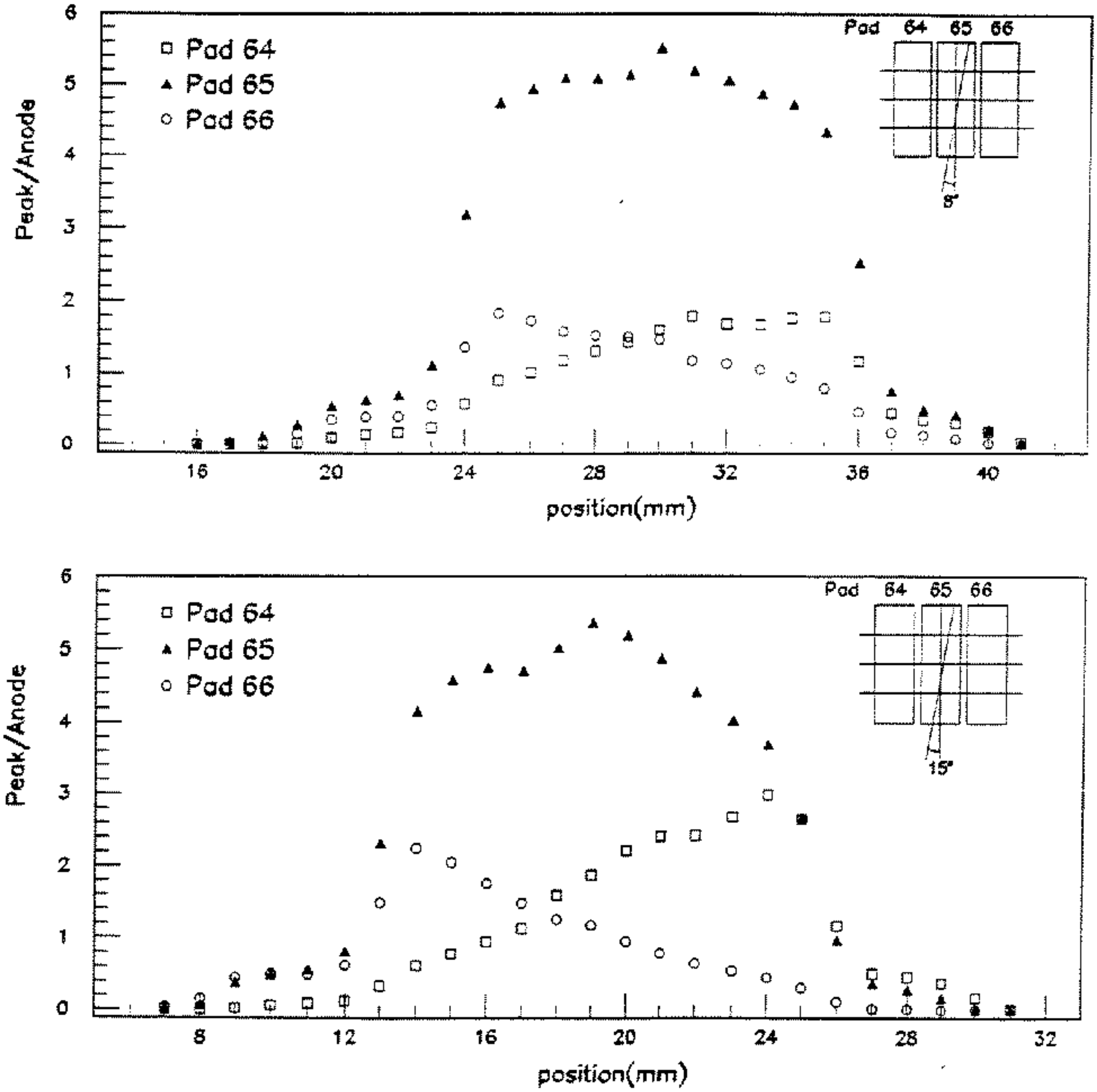

Figure 11: Pad response function with scan angles of 8 and 15 degrees for pads in the straight scetion of pad row.

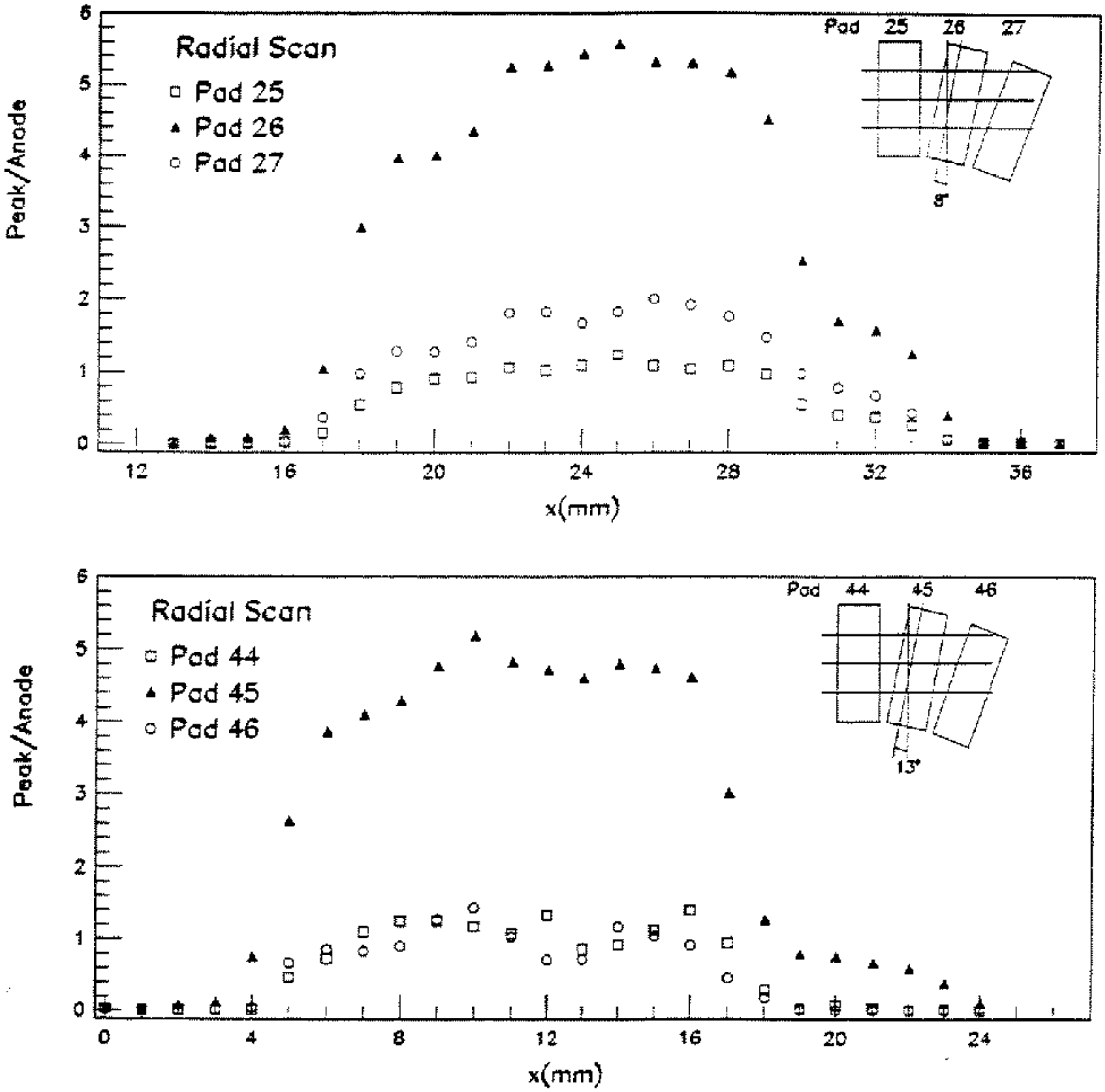

Figure 12: Pad response function with radial scan for pads in the circular scetion of the pad row.

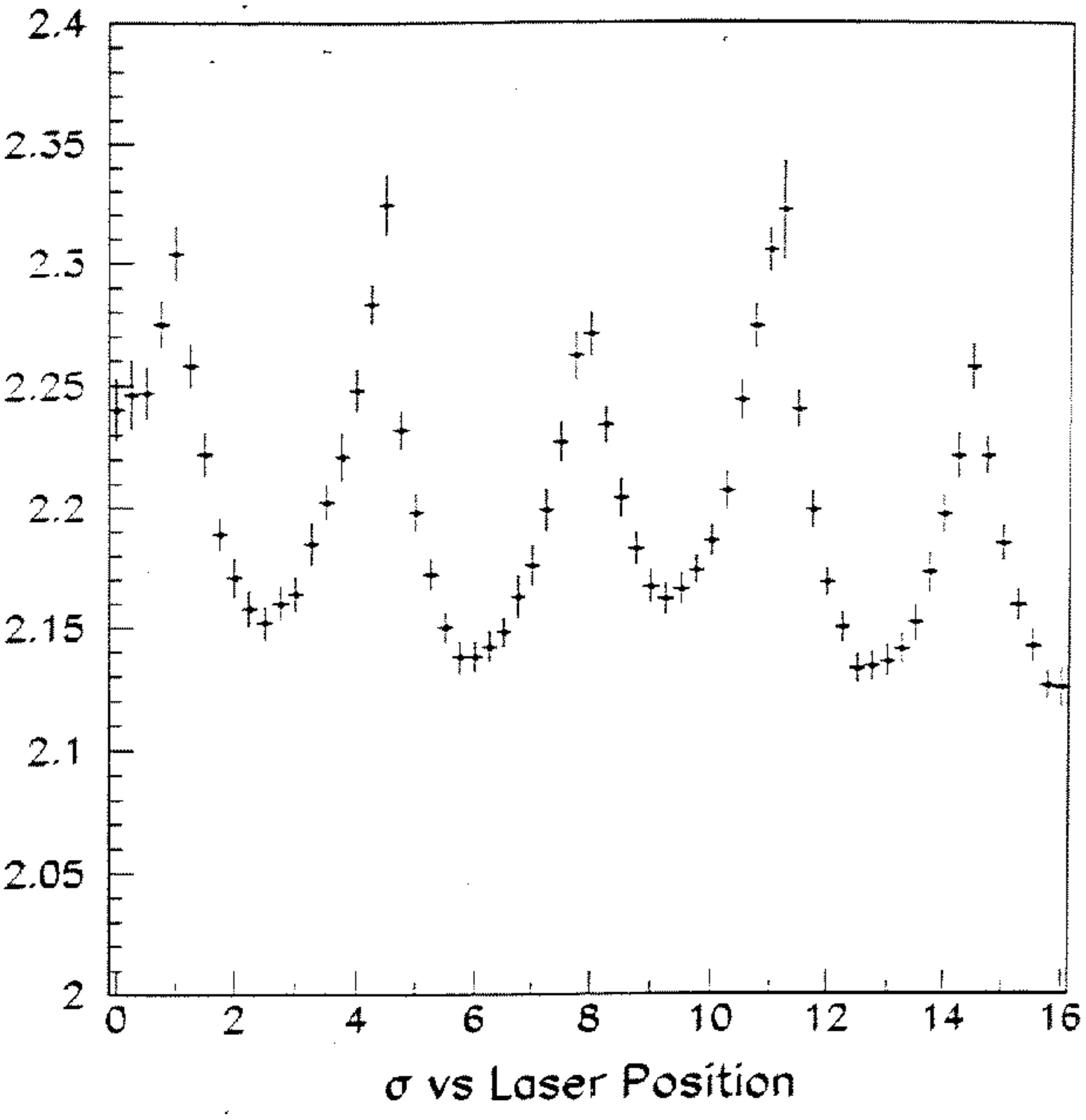

Figure 13: The width, σ, of the pad response function as a function of laser position measured from three pads.

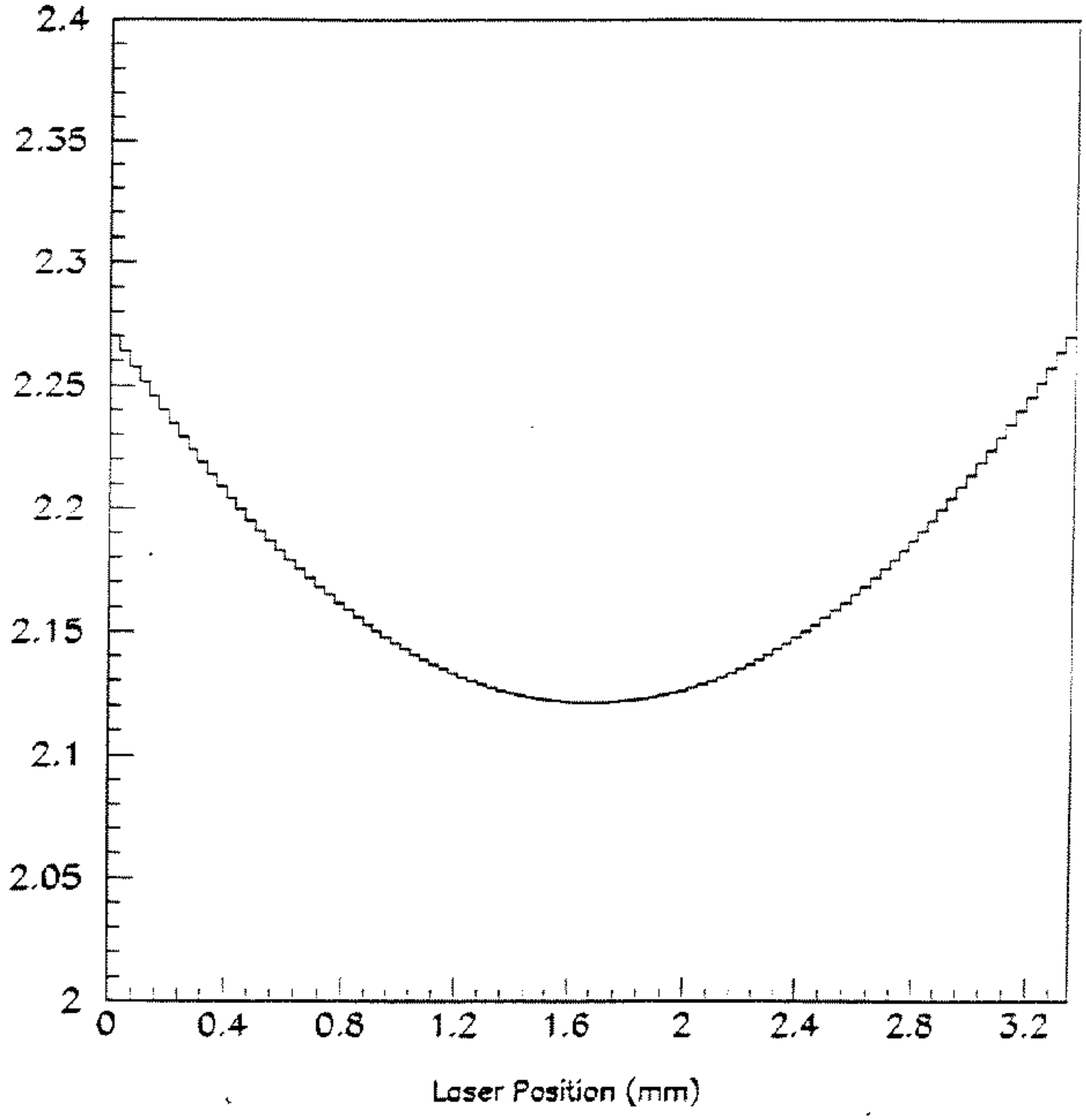

Figure 14: Expected width as a function of the avalanche position from the pad response function measurement as shown in figure 8.

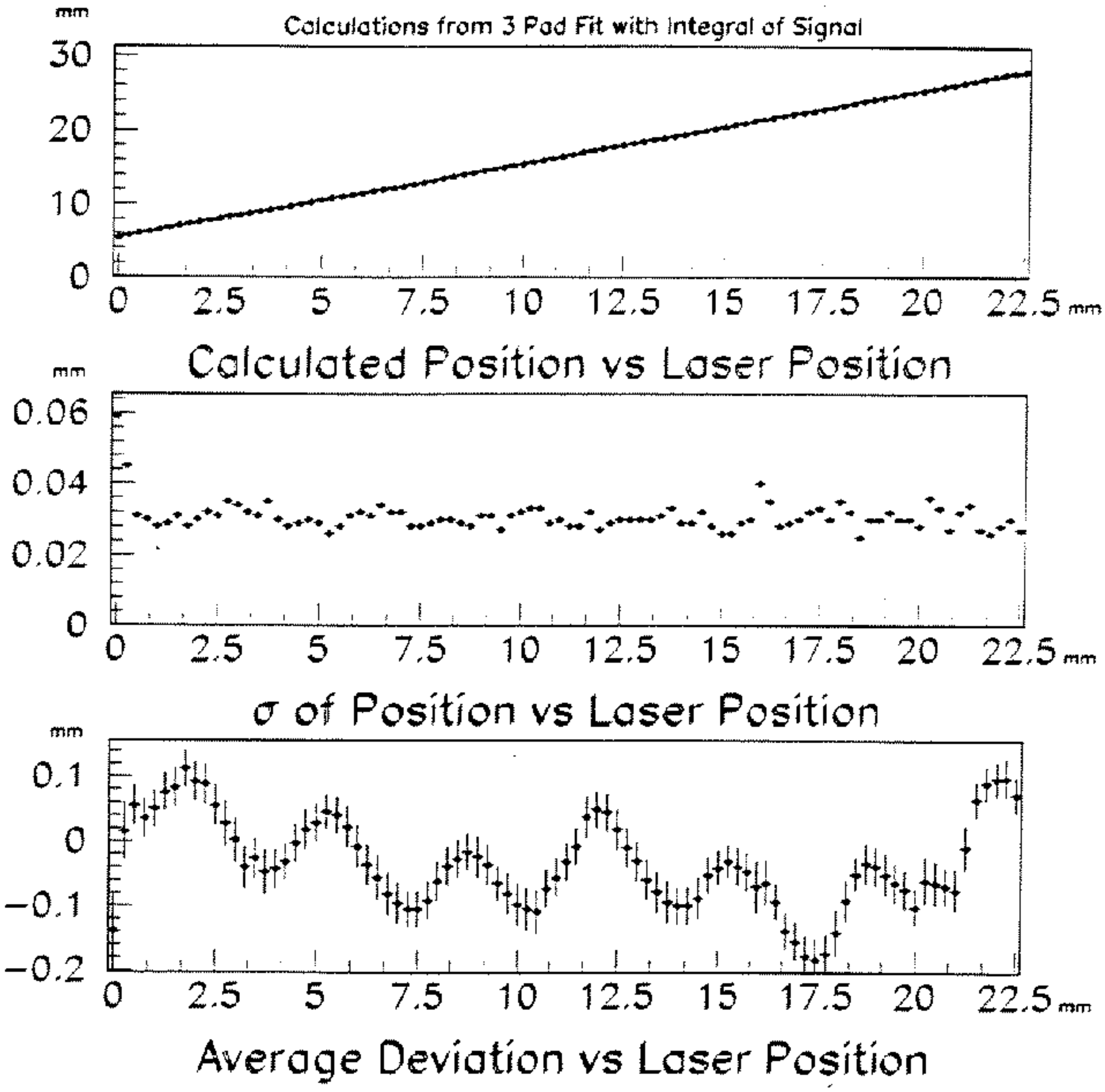

Figure 15: Calculated position, position resolution and position deviation as a function of the laser position for three pad fits.

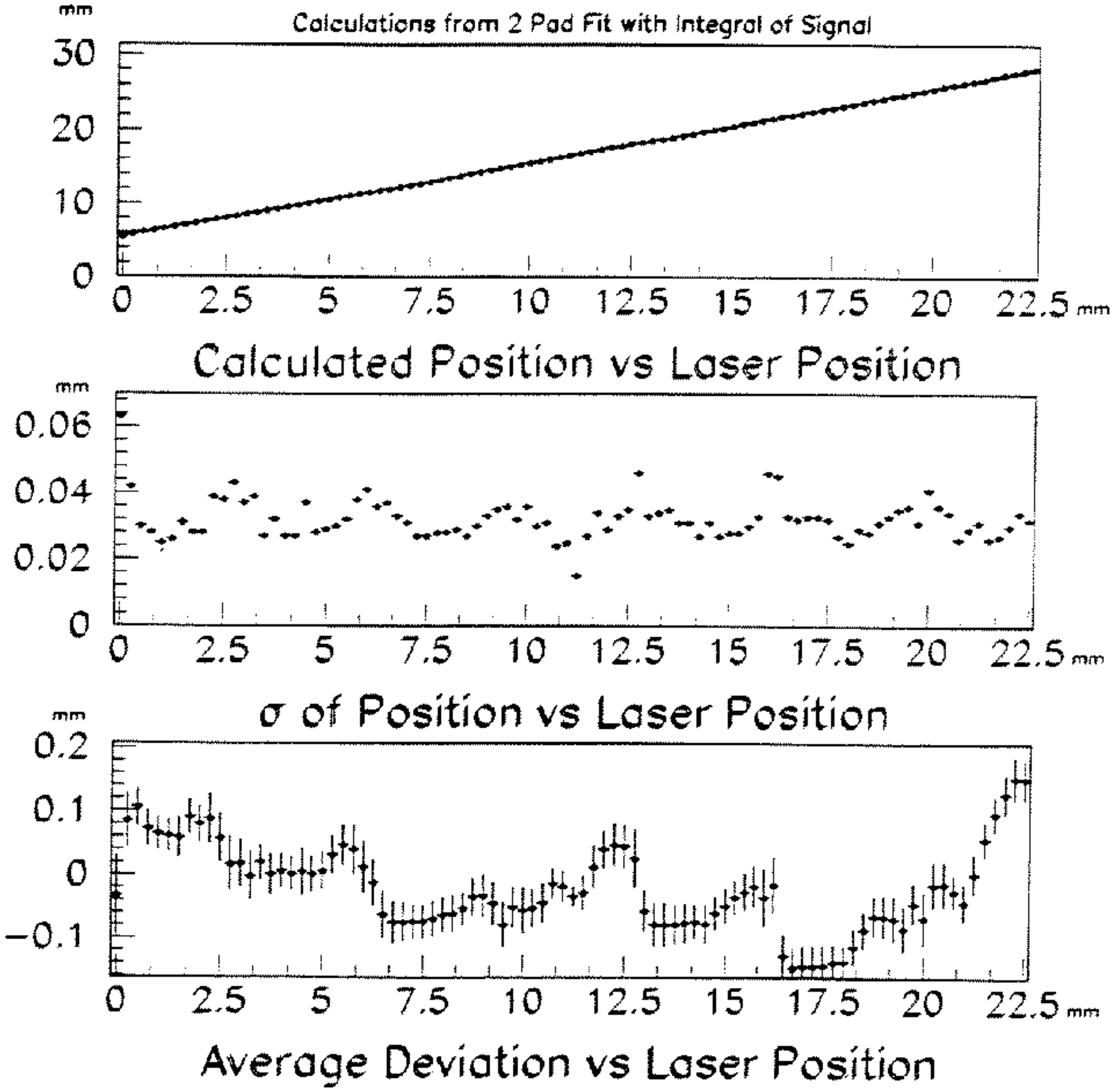

Figure 16: Calculated position, position resolution and position deviation as a function of the laser position for two pad fits.

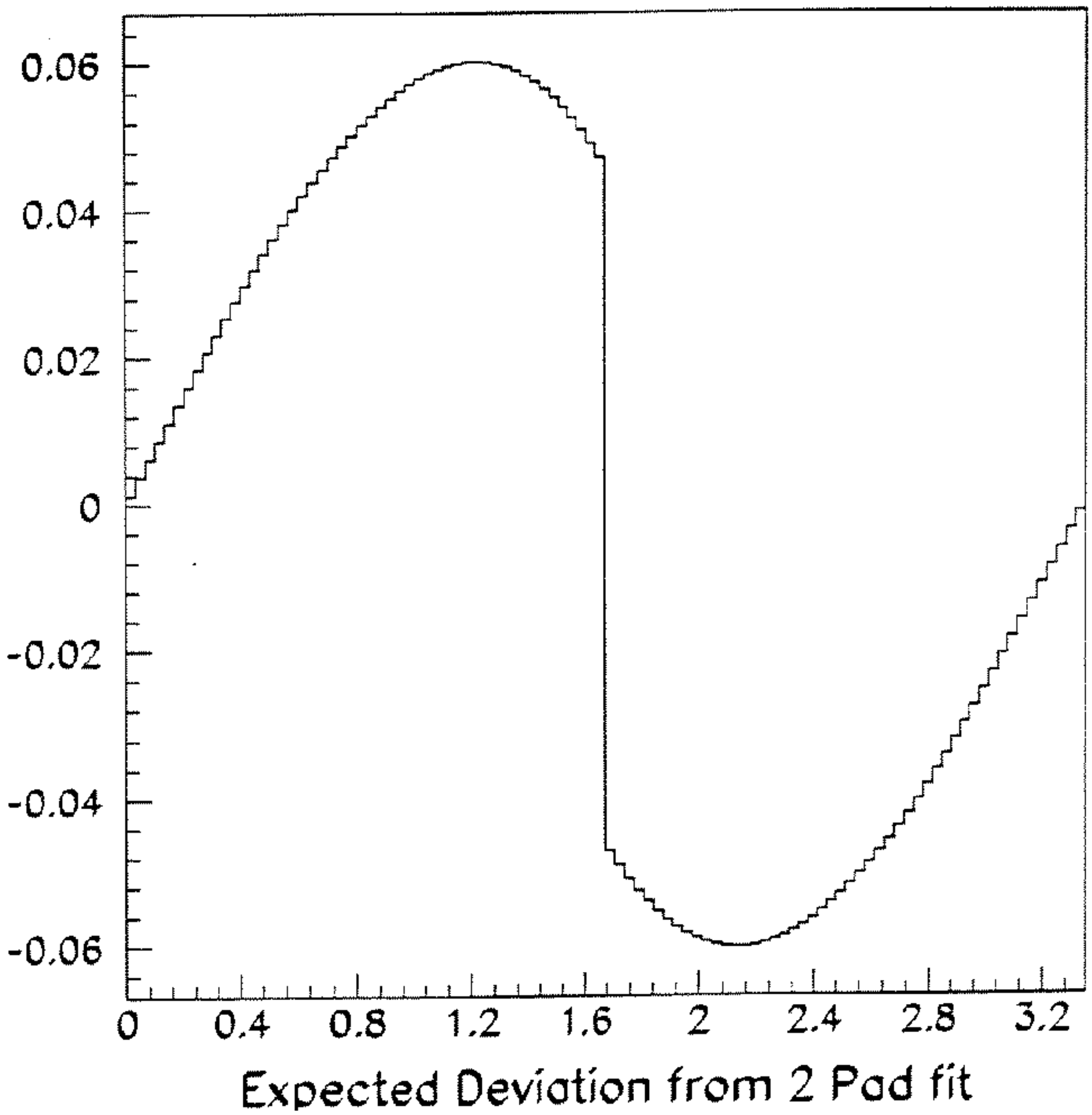

Figure 17: Expected position deviation as a function of the laser position for two pad fits.

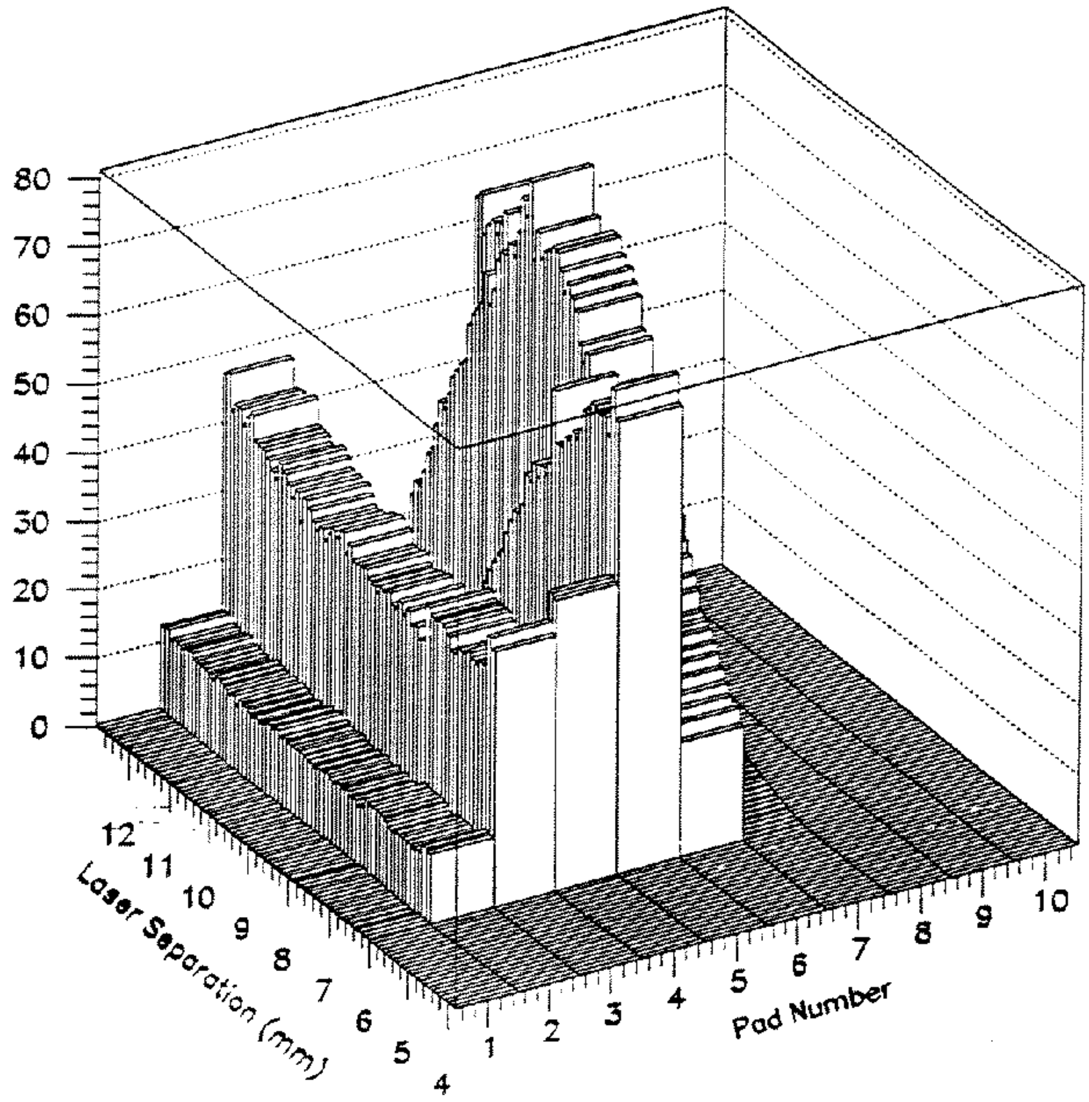

Figure 18: Lego profile of the pad amplitude as a function of laser separation. Note the intensities of the two lasers are camparable.

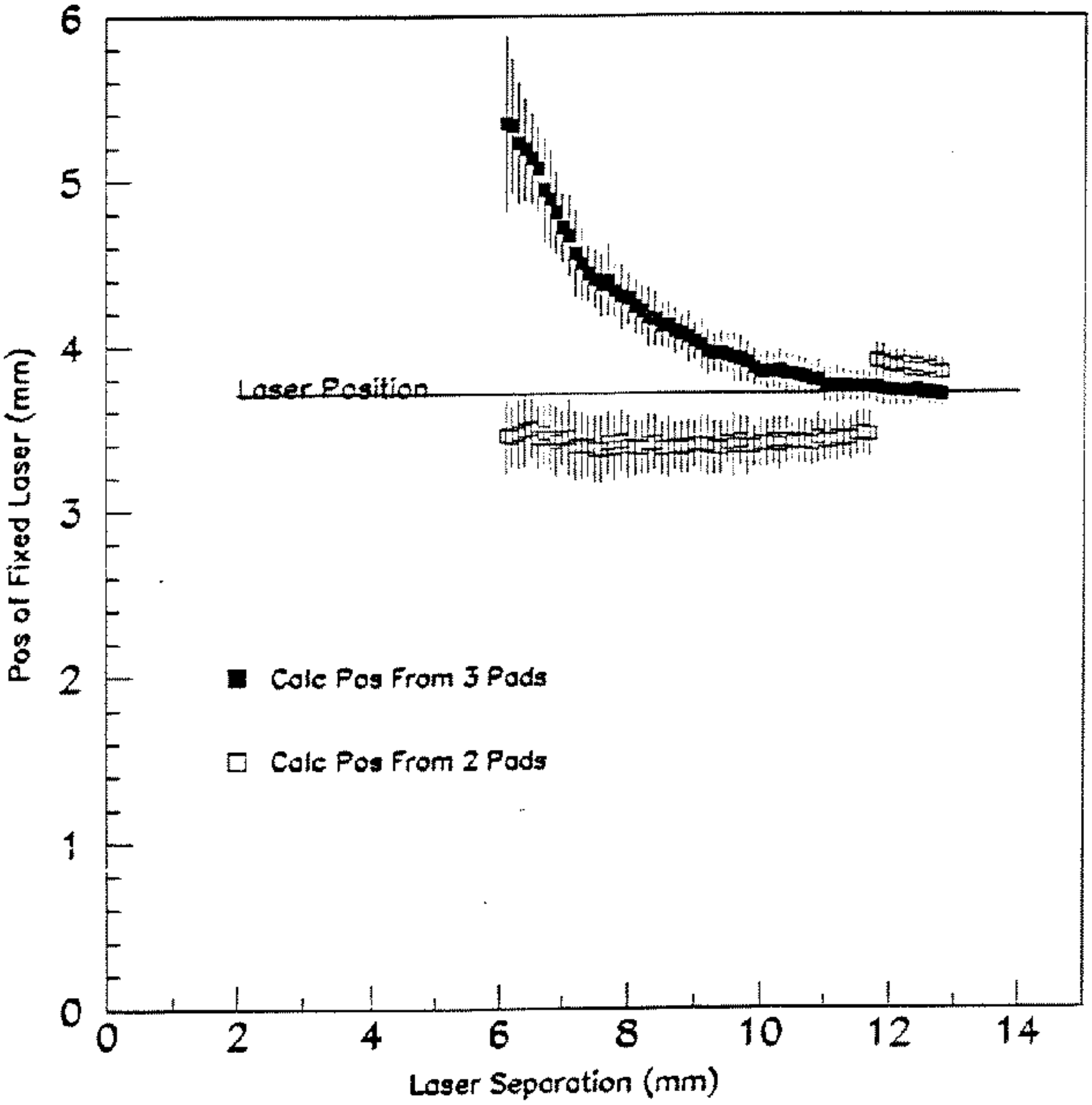

Figure 19: Position calculated from two and three pad fits for the fixed laser.

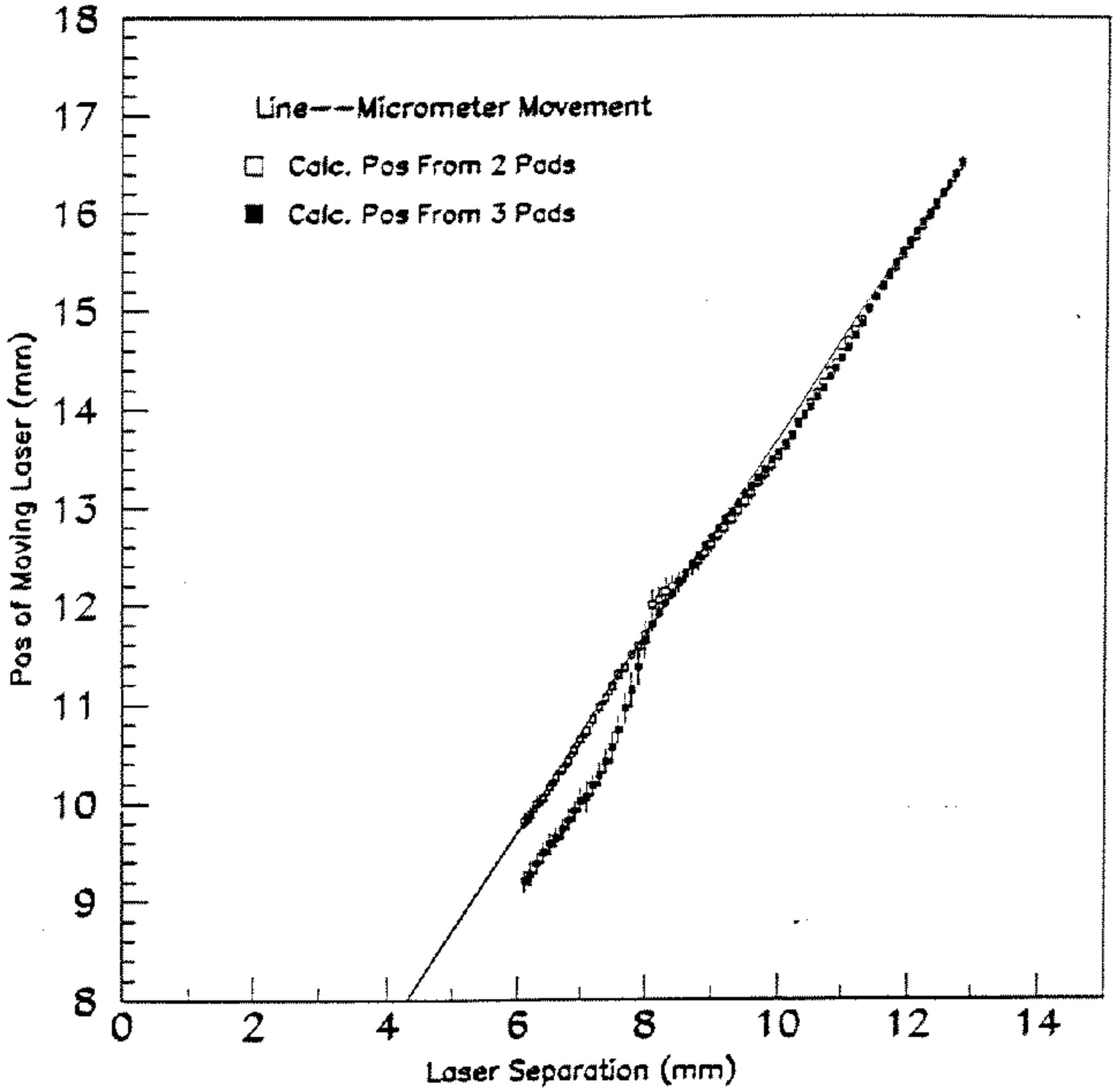

Figure 20: Position calculated from two and three pad fits for the moving laser.

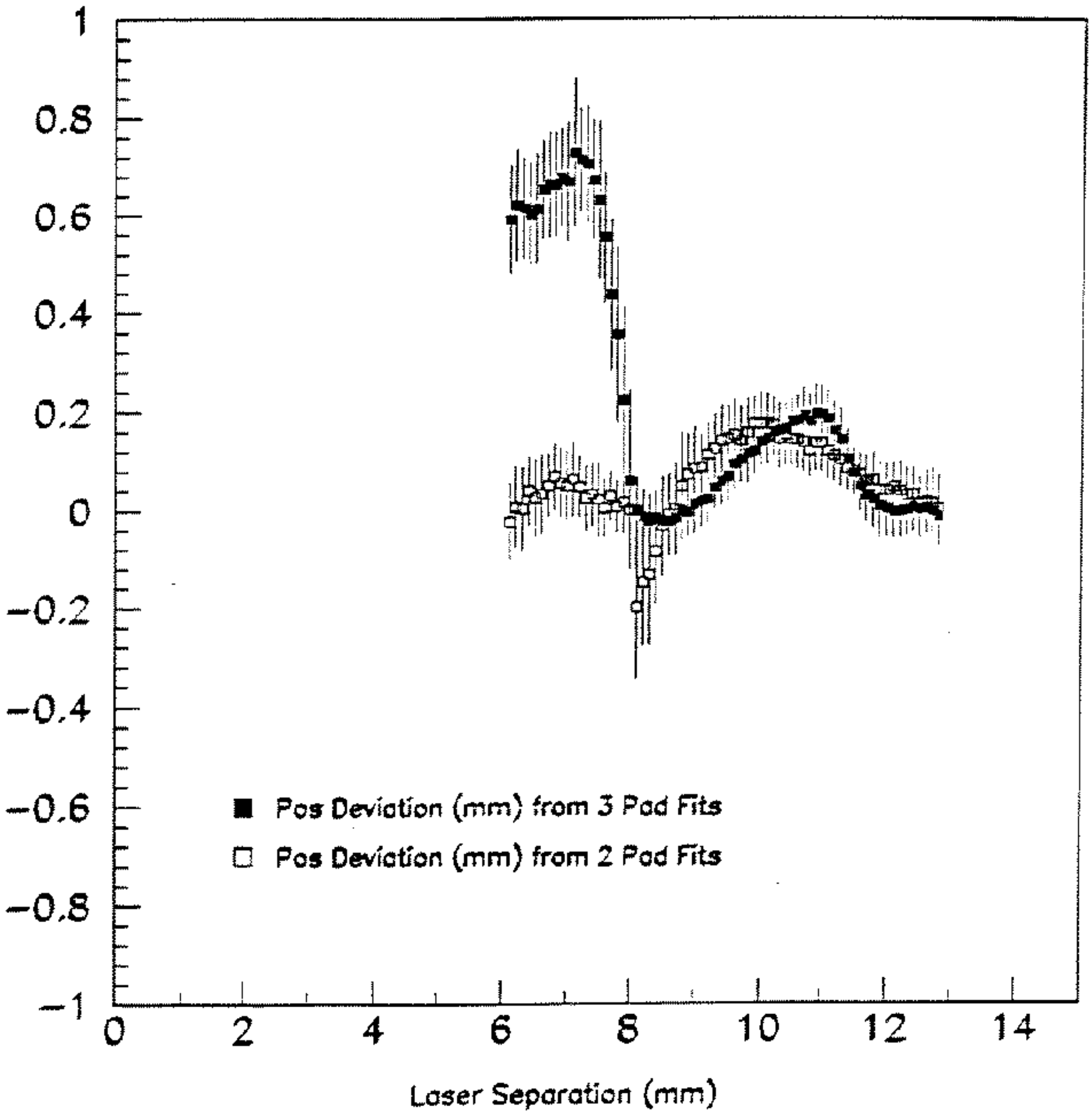

Figure 21: Position deviation as a function of the laser separation for the moving laser.

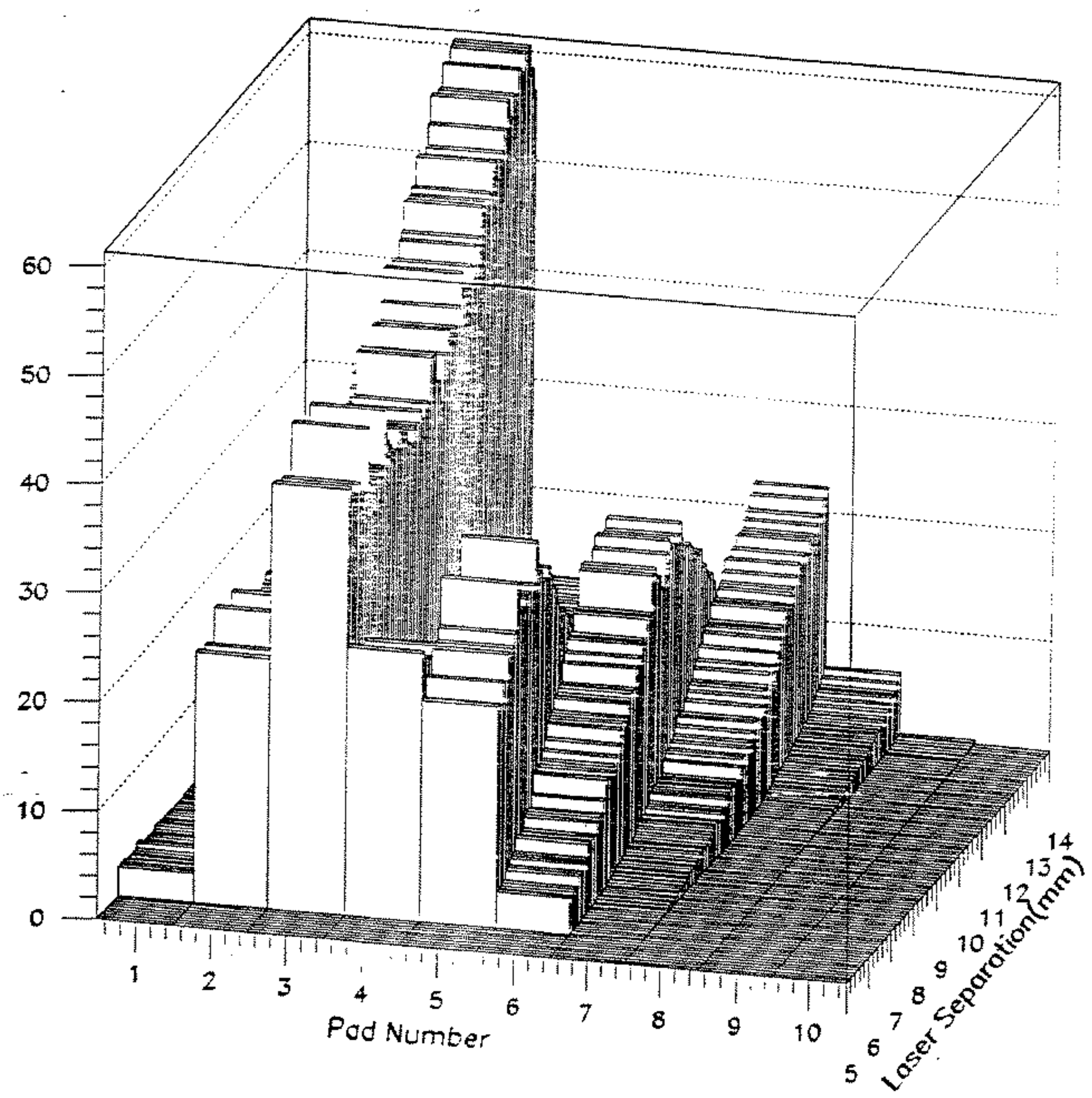

Figure 22: Lego profile of the pad amplitude as a function of laser separation for lasers with greatly different intensities.

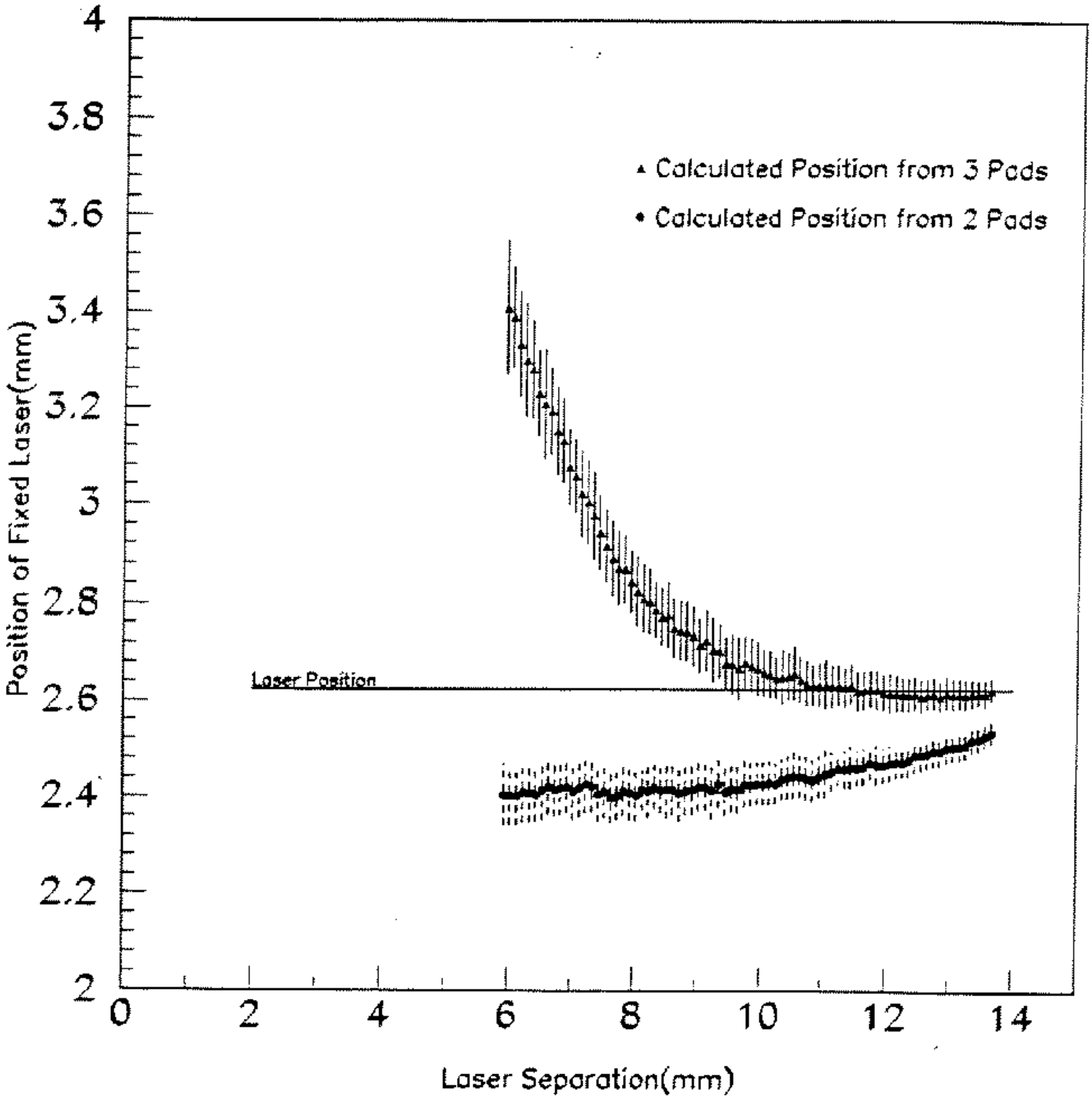

Figure 23: Calculated position for the fixed laser with strong intensity.

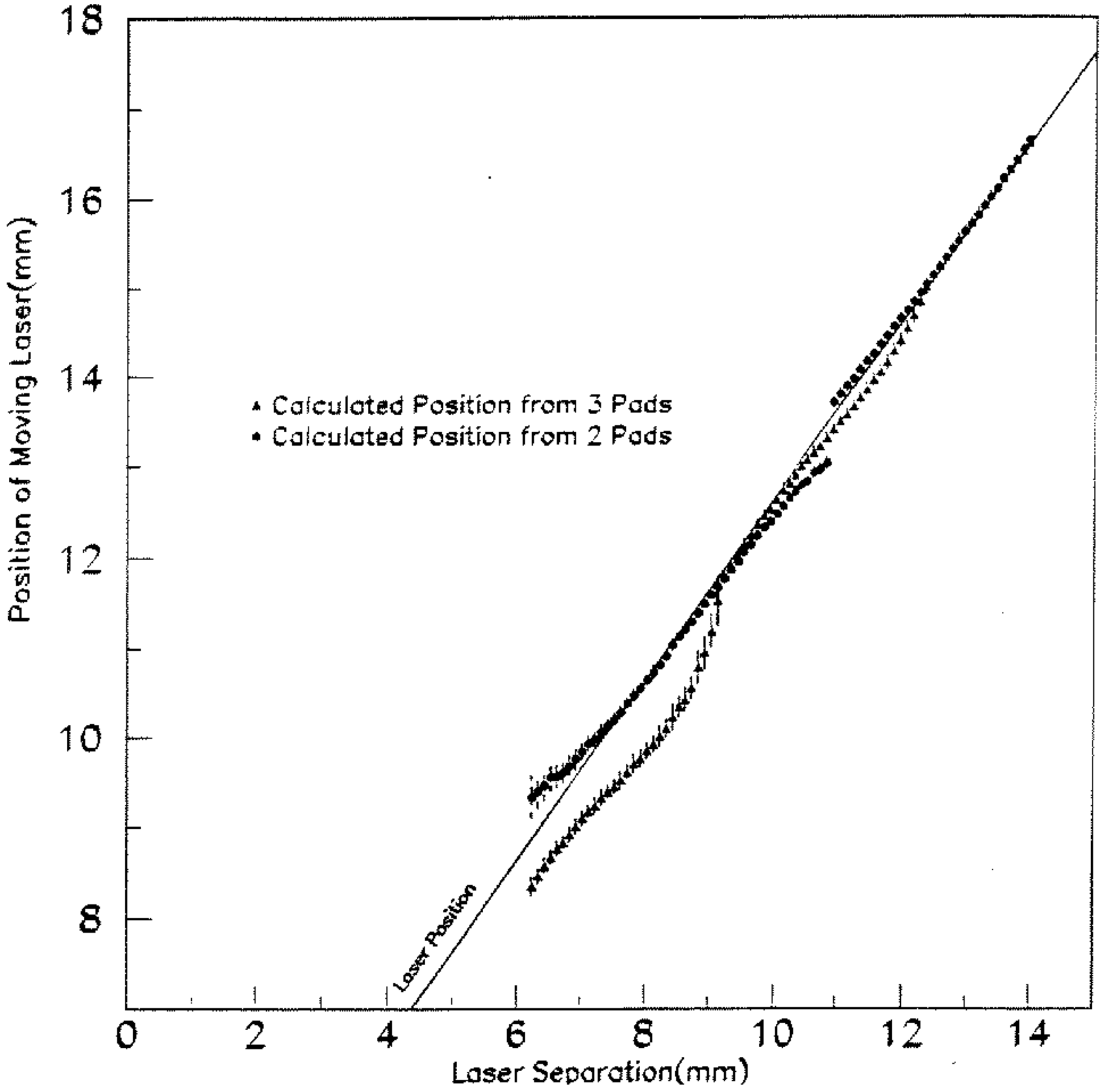

Figure 24: Calculated position for the moving laser with weak intensity.

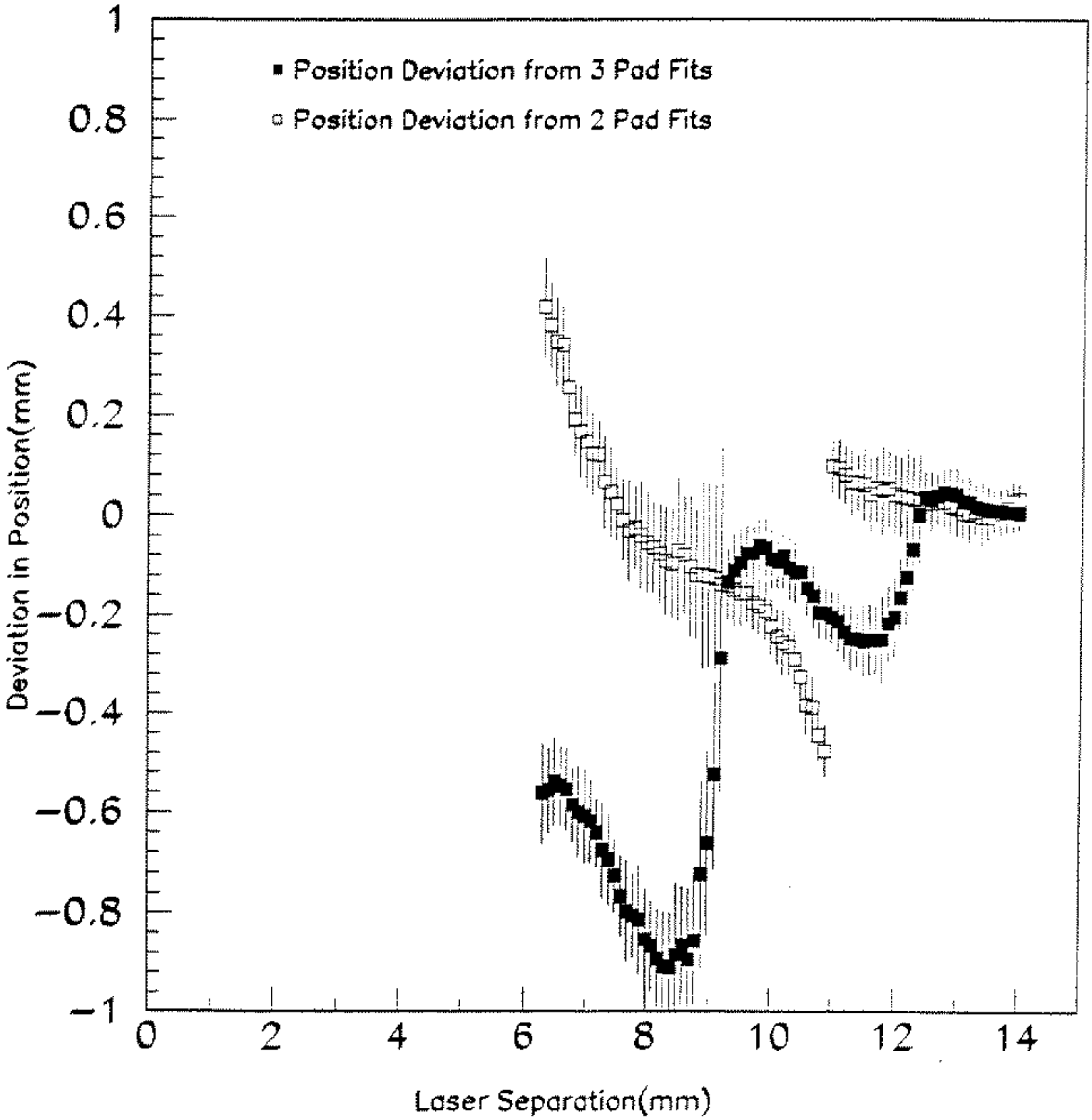

Figure 25: Position deviation for the moving laser with weak intensity. Note the two-track resolutin is reduced as compared with that in figure 21 due to stronger influence from the other laser.